CRREL
REPORT 85-9

US Army Corps of Engineers
Cold Regions Research & Engineering Laboratory

Thermal convection in snow

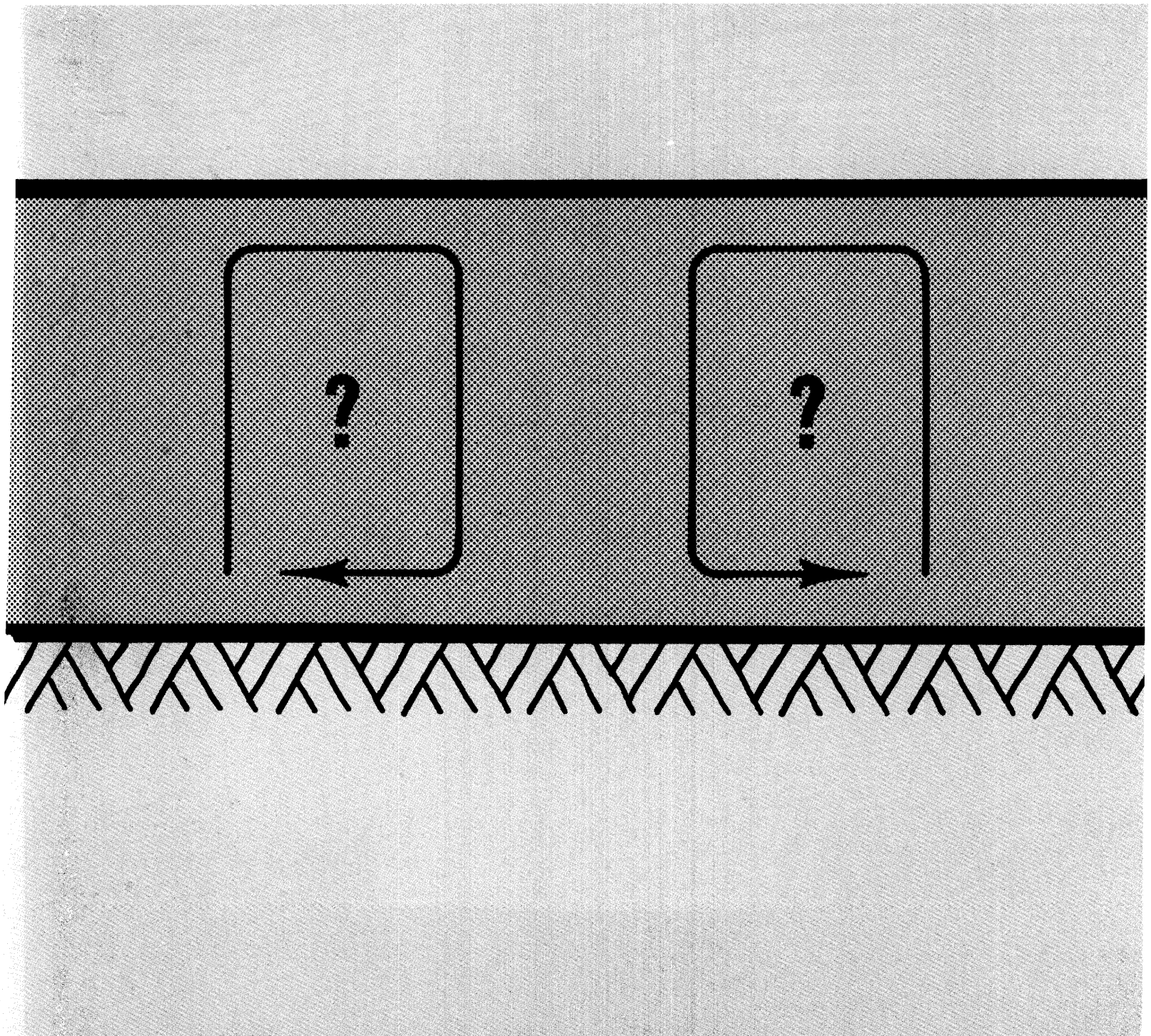

CRREL Report 85-9

May 1985

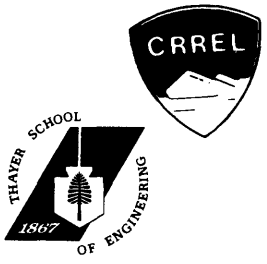

Thermal convection in snow

D.J. Powers, S.C. Colbeck and K. O'Neill

Prepared for
OFFICE OF THE CHIEF OF ENGINEERS

REPORT DOCUMENTATION PAGE

READ INSTRUCTIONS BEFORE COMPLETING FORM

1. REPORT NUMBER: CRREL Report 85-9	2. GOVT ACCESSION NO.
3. RECIPIENT'S CATALOG NUMBER	
4. TITLE (and Subtitle): THERMAL CONVECTION IN SNOW	5. TYPE OF REPORT & PERIOD COVERED
	6. PERFORMING ORG. REPORT NUMBER
7. AUTHOR(s): D.J.Powers, S.C. Colbeck and K. O'Neill	8. CONTRACT OR GRANT NUMBER(s)
9. PERFORMING ORGANIZATION NAME AND ADDRESS: U.S. Army Cold Regions Research and Engineering Laboratory, Hanover, New Hampshire 03755-1290	10. PROGRAM ELEMENT, PROJECT, TASK AREA & WORK UNIT NUMBERS: DA Project 4A161102AT24/C/EI/001
11. CONTROLLING OFFICE NAME AND ADDRESS: Office of the Chief of Engineers, Washington, D.C. 20314	12. REPORT DATE: May 1985
	13. NUMBER OF PAGES: 70
14. MONITORING AGENCY NAME & ADDRESS (if different from Controlling Office)	15. SECURITY CLASS. (of this report): Unclassified
	15a. DECLASSIFICATION/DOWNGRADING SCHEDULE

16. DISTRIBUTION STATEMENT (of this Report)

Approved for public release; distribution is unlimited.

17. DISTRIBUTION STATEMENT (of the abstract entered in Block 20, if different from Report)

18. SUPPLEMENTARY NOTES

19. KEY WORDS (Continue on reverse side if necessary and identify by block number)

Experimental data	Snow
Heat flux	Snow crystals
Mathematical models	Vapor flux

20. ABSTRACT (Continue on reverse side if necessary and identify by block number)

Large temperature gradients applied to a snow cover drive water vapor upwards and result in rapid recrystallization of snow crystals. The same temperature gradients create gradients of air density that can cause flows of air through the snow cover. The formalism necessary to describe these flows is developed here in an effort to include the convection of vapor in the understanding of snow metamorphism. The theory of convection through porous media is extended here to include the transport of water vapor, which is important because of its latent heat. Results are presented in terms of a Lewis number, defined as the ratio of thermal to mass diffusivities. For Lewis numbers greater than 1.0, phase change intensifies convection, and for Lewis numbers less than 1.0, phase change retards convection. Two boundary conditions of special interest in the study of snow, a constant heat flux bottom and a permeable top, are

20. Abstract (cont'd).

investigated. Their influence on the transfer of heat is quantified, and it is found that heat transfer can be described as a linear function of the driving force for convection. Convection in sloped layers is quantified, and explained in a physically consistent manner. The effect of a permeable top on convection at low Rayleigh numbers is derived. Experiments are performed to measure the effects of convection on heat transfer through glass beads and snow. The model results using constant flux boundary conditions are confirmed by the experiments. Experiments show that convection can occur in snow, and that convection behaves in a manner consistent with our theoretical understanding of the phenomenon. Some uncertainty exists about the permeability and thermal conductivity of snow and hence it is uncertain if thermal convection would occur for a given temperature gradient, density and thickness. Also, for a given convective intensity, there is much uncertainty about how much the rate of snow metamorphism is increased.

PREFACE

This report was prepared by Daniel J. Powers and Dr. Samuel C. Colbeck of the Snow and Ice Branch, Research Division, and Dr. Kevin O'Neill of the Geotechnical Research Branch, Experimental Engineering Division, U.S. Army Cold Regions Research and Engineering Laboratory. Daniel Powers was a graduate student at the Thayer School of Engineering at Dartmouth College throughout most of this study. The study was sponsored by DA Project 4A161102AT24/C/EI/001 *Mechanical Processes in a Snow Cover*.

This report was technically reviewed by Michael Ferrick and Dr. Jerome Johnson of CRREL. Edward Perkins was especially cooperative with drafting and Donna Harp with typing during the initial stages of preparation. Horst Richter of Thayer School and Dr. Wilford Weeks of CRREL reviewed earlier versions of the manuscript.

CONTENTS

ILLUSTRATIONS

Figure

TABLES

NOMENCLATURE

a	Dimensionless wavelength
AR	Aspect ratio
B	Parameter in equation of state for vapor
C	Heat capacity
d	Grain diameter
D	Mass diffusivity
g	Acceleration of gravity
Gr	Grashof number
h	Enthalpy
H	Depth of porous layer
j	Diffusional mass flow
K	Intrinsic permeability
k	Thermal conductivity
L	Latent heat of sublimation
Le	Lewis number
Nu	Nusselt number
p	Pressure
q	Heat flux
Ra	Rayleigh number
Sh	Sherwood number
t	time
T	Temperature
u	x direction velocity
U	Internal energy
V	Specific volume
v	Velocity vector
W	Cell dimensions
w	z direction velocity
x	Horizontal coordinate
z	Vertical coordinate
β	Isobaric coefficient of thermal expansion
ΔT	Characteristic temperature difference
κ	Thermal diffusivity $[k_m/(\rho Cp)_f]$
μ	Viscosity
π	3.14159.....
ρ	Density
τ	Viscous stress tensor
ϕ	Angle from horizontal
ψ	Stream function
Δt	Time step
ϵ	Porosity

Subscripts

a	Air
eff	Effective of macroscopic quantity
m	Property of porous media, fluid and solid
i	Component i or node i
j	Component j or node j
f	Fluid property
c	Conduction only
p	Constant pressure
T	Constant temperature
v	vapor
s	Snow
o	Reference value
cr	Critical value

Superscripts

$'$	Dimensional quantity later made nondimensional
$\rightarrow$	Vector
$=$	Tensor
ℓ	Time step level

THERMAL CONVECTION IN SNOW

D.J. Powers, S.C. Colbeck and K. O'Neill

INTRODUCTION

The size and shape of grains and the density of snow greatly affect all of its material properties. Snow covers of similar density and grain size may have widely different crystal shapes, ranging from rounded to sharply angular. The range over which the physical properties vary is quite large.

It is widely known that when a low density dry snow is subjected to a temperature gradient of at least 0.1°C/cm, many of the grains will develop facets. A dramatic loss of strength usually accompanies this rapid recrystallization and this strength loss is commonly thought to be a factor in the release of avalanches. Efforts to model crystal growth in snow have so far focused solely on vapor diffusion among the crystals. However, the temperature gradients that drive the diffusion of water vapor also establish air density gradients that may lead to convective flows of air. These flows, if they occur, would certainly have a large impact on the flux of heat and vapor and therefore might affect the metamorphism of snow.

Snow metamorphism

Dry snow metamorphism is often classified as equitemperature or temperature gradient. The first term refers to conditions under which grains become more rounded and sintering processes increase the size of bonds between grains. It is now recognized that these processes do not ever occur under isothermal conditions, as the name would imply. Furthermore, when nature imposes even a slight gradient on the snow cover the processes are greatly accelerated. Colbeck (1982) refers to the rounded grains as the equilibrium form, which is probably a better description than equitemperature.

Temperature gradient metamorphism is characterized by the growth of large angular or faceted crystals. Actually, temperature gradient metamorphism is also a misnomer, since large faceted crystals occur only when *large* temperature gradients are applied to low density snow. A loss of strength frequently accompanies the growth of large faceted grains, especially when hollow depth hoar crystals form. These grow most readily in low density snows subjected to very large temperature gradients. More solid faceted crystals grow at lower temperature gradients, or in higher density snows (Akitaya 1974, Marbouty 1980).

Mass transfer by diffusion in snow

Here we are primarily concerned with metamorphism driven by strong temperature gradients because the temperature gradients that drive depth hoar growth could also drive the convective flows that are the subject of the present work.

Metamorphism in dry snow occurs by the transport of water vapor. Vapor diffuses from areas of high vapor density to low vapor density, or it may be carried by convective currents of air. In

this section, we discuss only the diffusion process. Vapor pressure gradients exist in snow because of temperature gradients or curvature differences, or both. Vapor pressure is higher over warmer ice and over convexly curved ice. When temperature gradients are low, curvature effects are important, and concave sections will begin to fill in by vapor deposition. However, at the large values of temperature gradient where depth hoar grows, curvature effects are negligible, and the transport of vapor is governed by the temperature field. Strong gradients occur for prolonged periods most commonly in cold climates with shallow snow covers (less than 100 cm).

If we think of a vertical coordinate as positive upwards, the gradient will be negative. Henceforth, a large gradient refers to a large absolute value of the negative gradient.

Early attempts to model depth hoar growth (i.e., Giddings and LaChapelle 1962) used a one-dimensional diffusion equation to describe the flux of vapor through dry snow:

$$j_z = -D \frac{\partial \rho_v}{\partial z} \tag{1}$$

where D is a diffusion coefficient. Giddings and LaChapelle tried to calculate crystal growth rates assuming that all vapor stopped at one level. This assumption is generally meaningless, although eq 1 can be used to represent mass fluxes in one dimension. Experimental data from Yosida (1955) and Yen (1963) show a rate of vapor transport four or five times greater than the Giddings and LaChapelle model predicts. Yosida formulated his results in an equation similar to eq 1, using an effective diffusivity coefficient to describe the flux of vapor. He found D_{eff} equal to 0.85 cm^2/s and invariant with snow density over the range of $0.08 < \rho_s < 0.51$ g/cm^3. Yen confirmed these results, although he tested only densities in the range of $0.38 < \rho_s < 0.48$ g/cm^3. Trabant and Benson (1972) calculated flux rates in the field and found them to be about an order of magnitude greater than they calculated using eq 1. Although they did not calculate an effective diffusivity, their results indicate an effective diffusivity about a factor of 2 greater than that of Yosida.

The reason for the high observed flux rates is not entirely clear. Trabant and Benson suggest that thermal convection may be important, and this may certainly be part of the answer. In Yosida's experiments the geometry would make convection unlikely. The common observation of rapidly growing depth hoar in shallow layers of snow where convection is unlikely also points to the need for some other explanation for the high flux rates.

Yosida supposed that vapor transport occurred by a "hand-to-hand" mechanism, i.e., that mass was transferred by diffusion from grain to grain and not along vertical air channels. Since ice is a much better conductor than air, temperature gradients in the air spaces may be much higher than the average gradient in the snow, and thus local fluxes may be much higher than that predicted on the basis of an average temperature gradient. This is part of the explanation for the high values of D_{eff}. Colbeck (1983) quantified this effect in an effort to model grain growth. His model did show reasonable growth rates, although he was forced to arbitrary assumptions about snow stereology because of a lack of good data. His model has not been applied to calculate macroscopic mass flux rates, and thus it is not yet certain just what the quantitative effects of hand-to-hand transfer are on those mass fluxes.

Colbeck's model showed that grain growth is primarily attributable to a coupling between vertically aligned particles, just as Yosida suggested. The rate of mass movement between the particles is equal to the rate of mass gain by the growing particle. Thus grains do not grow because of a macroscopic redistribution of mass between regions of the snow cover as described in some flux divergence models. The particle-to-particle mechanism explains the experimental observation of rapid grain growth without significant snow density change (Marbouty 1980). The relatively intense vapor transport between coupled grains is included in the overall macroscopic vapor flux described by eq 1, with an effective diffusion coefficient. We study the macroscopic fluxes and their possible enhancement by convection in order to see how the convective fluxes affect the grain-scale vapor transport that controls snow metamorphism.

Heat transfer

Typically, heat transfer through snow is modeled by a conduction equation of the form

$$q_z = -k \frac{\partial T}{\partial z} \tag{2}$$

where k is a thermal conductivity. It is customary to use an effective thermal conductivity to account for the heat conduction through both the fluid and solid in porous media. In snow we must also consider the latent heat carried by the flux of vapor. The transport of heat ascribable to vapor diffusion is given by

$$q_{vz} = -L D_{eff} \frac{\partial \rho_v}{\partial T} \frac{\partial T}{\partial z} \tag{3}$$

where L is the latent heat of sublimation.

Since this flux is also proportional to the temperature gradient, all contributions to heat flow may be lumped into an effective thermal conductivity, as described by eq 2. Data on these effective thermal conductivities, summarized by Mellor (1977), show a great deal of scatter for any given density. In part this may be attributable to the temperature dependence of the vapor term. The experimental data of Pitman and Zuckerman (1967) show the expected trends with temperature; however, the magnitude of the change in k_{eff} with temperature that they observed is too great to be explained by the temperature dependence of the vapor diffusion term.

A basic understanding of the relative contributions of conduction through ice, of conduction through air and of vapor diffusion to the total transport of heat is lacking. Generally, it is assumed that conduction through the air is negligible, since the thermal conductivity of air is 100 times less than that of ice. However, the aforementioned notion of exaggerated gradients in the voids between particles, coupled with the high porosity of snow, leads us to estimate that the conduction of heat through the air spaces may be on the order of 10% of that through the ice lattice.

The contribution of vapor transport can be estimated from eq 3, defining k_v as the vapor diffusion equivalent of thermal conductivity, or

$$k_v = L D_{eff} \frac{\partial \rho_v}{\partial T} . \tag{4}$$

where k_v is a function of temperature, as illustrated in Figure 1. At 0°C, using Yosida's D_{eff} of 0.85 cm^2/s, we find $k_v = 2.4 \times 10^{-4}$ cal/cm^2 s °C. Since total thermal conductivities of less than this are observed, we must be somewhat skeptical of either Yosida's notion that D_{eff} is not a function of density, or of the thermal conductivity data (or of both). It is reasonable that D_{eff} is a function of density, since crystal growth rates are strongly dependent on snow density.

In summary, for lower density snows, conduction through air is probably not negligible, while the transfer of latent heat is probably very important. In higher density snows, where the total thermal conductivity is greater, the po-

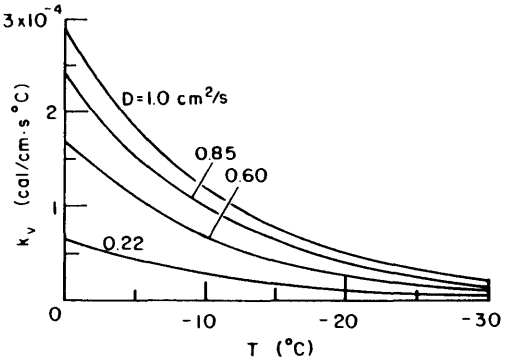

Figure 1. Contributions of vapor diffusion to heat transport in terms of thermal conductivity k_v *for various values of effective diffusivity* D.

rosity is less and temperature differences among neighboring grains are less, conduction through the ice lattice may dominate the heat transfer process.

BACKGROUND–POROUS MEDIA

This section examines the developments that have taken place in the study of thermal convection in porous media. The impetus for much of this work has been an interest in petroleum and geothermal reservoirs. However, much of the work is of a basic nature, and may be applied to snow. The aim here is to outline the fundamental principles that govern thermal convective flows in porous media and to summarize the pertinent results.

Structure of thermal convection

Convective flows occur when buoyancy forces, driven by density gradients, are sufficient to overcome viscous drag. As warm air rises, cold air from above must descend for continuity. Thermal convection can thus be thought of as nature's way of trying to relieve unstable density gradients.

Circulation patterns in a horizontal layer heated from below appear commonly in two forms. One form, commonly called two-dimensional convection, consists of rolls (see Fig. 2) that are very long in one direction, and are roughly equal in the other two dimensions. The other form is three-dimensional convection, in which the cell takes a hexagonal pattern when viewed from above. The cell size at the onset of convection was calculated for both forms by Combarnous and Bories (1975) (Fig. 2).

When the porous layer is confined laterally, the dimensions of the convective cells are governed by the dimensions of the container. Beck (1972), and Tewari and Torrance (1981) have predicted the preferred cell size at the onset of convection as a function of container dimensions for the closed-top and open-top cases respectively. Cheng (1978), in his review paper, draws two general conclusions about the results of Beck, and these seem to apply equally well to the results of Tewari. First, when one of the lateral dimensions is less than the vertical dimension, two dimensional convection is the rule. Secondly, the number and direction of rolls is governed by the tendency for the width of the roll to be nearly equal to its height. We can also say that when the upper boundary is permeable the lateral dimensions of the convective cell are about one and one-half times greater than for the closed top case, all other things being equal.

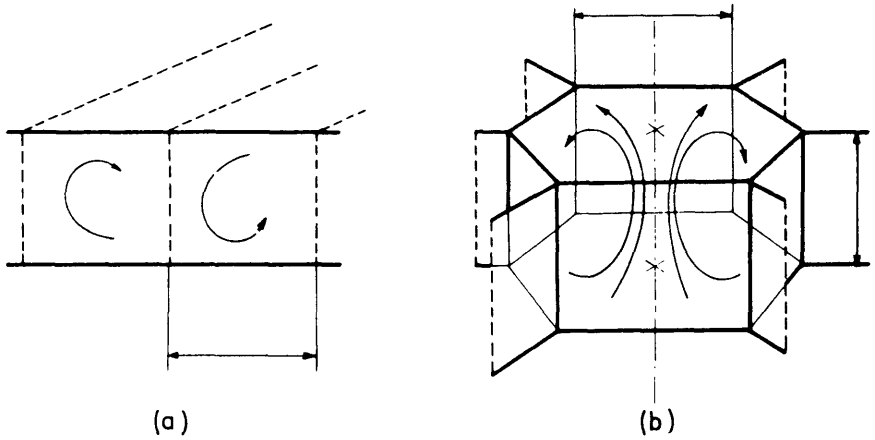

Figure 2. Longitudinal roll and hexagonal cell (after Combarnous and Bories 1975).

The above results strictly apply only at the onset of convection. When convection is "mild," these results are probably a good approximation. However, as convection intensifies, the preferred cell size can be greatly reduced. Numerical experiments by Straus and Schubert (1979) show that for random initial conditions, either two- or three-dimensional convection can occur. The mode that would maximize heat transfer is not necessarily the one that results.

Rayleigh number

The flow of fluids through a porous medium is described by Darcy's law, which is an empirical relation developed by Darcy from his classic set of experiments. Two assumptions are made here: that the fluid is Boussinesq, meaning that variations in fluid properties are negligible except where buoyancy terms are involved, and that it is incompressible, which implies that density will not vary directly as a result of the flow.

From a nondimensional form of Darcy's law (derived more completely in the *Modeling* section) comes an important nondimensional parameter known as the Rayleigh number, defined as

$$\mathrm{Ra} = \frac{\rho_o g \beta \Delta T H K}{\mu \kappa} \tag{5}$$

where κ is $k_m/(\rho C_p)_f$ and ρ_o is the fluid density at a reference temperature. The Rayleigh number, along with the boundary conditions, governs both the onset of convection and its intensity.

The definition of the temperature difference in the Rayleigh number depends on the thermal boundary conditions at the upper and lower surfaces. When the boundary conditions are constant temperatures at both upper and lower surfaces, then the ΔT is just the difference between those temperatures. However, we are also interested in lower boundaries with a constant heat flux (q). When this is the case, we define the temperature difference as qH/k_m, which is the temperature difference that would be observed if convection were absent.

Onset problem

Convection takes place when buoyancy forces are sufficient to overcome viscous resistance. For a porous medium, this happens when the Rayleigh number is sufficiently large. The critical value of the Rayleigh number at which convection begins is a function primarily of the boundary conditions. The critical Rayleigh number was originally calculated for a horizontal layer with isothermal, impermeable boundaries by Lapwood (1948). Nield (1968) has applied the analysis of Lapwood to other boundary conditions, including permeable or constant heat flux boundaries. Some of his results, pertinent to the present problem, are listed in Table 1, along with the results of the original problem considered by Lapwood.

Table 1. Summary for the onset of convection. After Nield (1968).

Case	*Top boundary*	*Bottom boundary*	Ra_{cr}	a_{cr}
1	Constant temperature, impermeable	Constant temperature, impermeable	39.5	3.14
2	Constant temperature, permeable	Constant temperature, impermeable	27.1	2.33
3	Constant temperature, impermeable	Constant flux, impermeable	27.1	2.33
4	Constant temperature, permeable	Constant flux, impermeable	17.7	1.75

The critical Rayleigh number is minimized for a given set of boundary conditions at some optimum cell size. The critical wave number a_{cr} is also given in Table 1. This wave number is defined as

$$a_{cr}^2 = \ell^2 + m^2$$

where ℓ and m are the wave numbers in the x and y directions, defined respectively as $\ell = 2\pi H/W_x$ and $m = 2\pi H/W_y$; W_x and W_y are the cell dimensions in the x and y directions respectively. Knowing a_{cr}, we can predict the cell size at the onset of convection for either two-dimensional rolls or three-dimensional hexagons.

The above results apply when the lateral extent of the layer is large. When confinement is important, the dimensions of the container dictate the cell form and the critical Rayleigh number. Beck (1972) and Tewari and Torrence (1981) solved for the cell form and critical Rayleigh number as a function of container size for the closed and open top cases respectively. They found that unless both the container dimensions are much less than the critical wavelengths, the critical Rayleigh number is not increased significantly. We also conclude that when one of the lateral dimensions is less than the critical wavelength, the preferred cell form at the onset is two-dimensional rolls.

Heat transfer attributable to thermal convection

When the Rayleigh number increases beyond the critical value, convection occurs, causing a significant increase in the rate of heat transfer. Numerical, analytical and experimental methods have all been used to investigate this phenomenon. Published results are commonly presented in terms of the Nusselt number, defined as

$$\mathrm{Nu} = \frac{k_{eff}}{k_m} \tag{6}$$

where k_{eff} is an effective thermal conductivity that accounts for both conductive and convective heat transfer. If Nu = 1.0, convection has no effect on heat transfer, whereas if Nu = 2.0, the

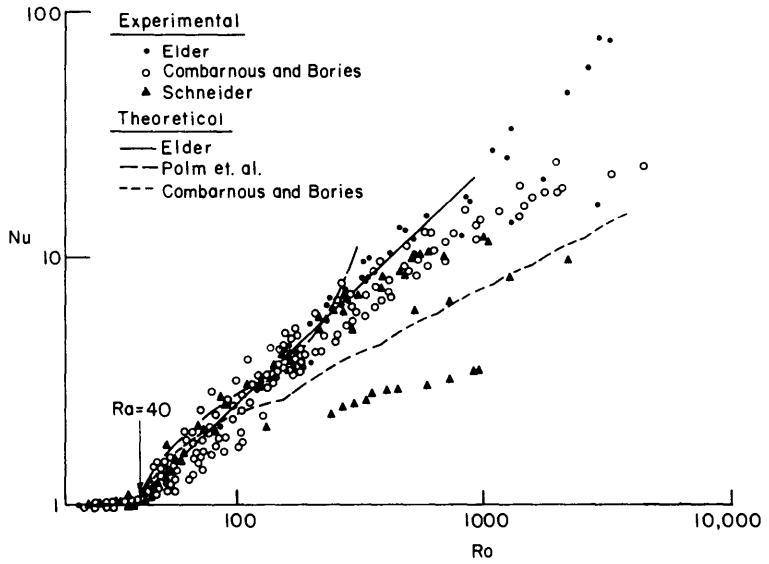

Figure 3. Experimental and theoretical results for heat transfer between isothermal, impermeable boundaries.

Table 2. Summary of the results of Ribando (1977), indicating the influence of constant flux bottom and permeable top boundary conditions.

Boundary conditions					
Top	*Bottom*	*AR*	*Ra*	*Nu*	ψ_{max}
Constant temperature, impermeable	Constant temperature, impermeable	0.6	200	4.07	6.87
Constant temperature, permeable	Constant temperature, impermeable	0.6	200	6.38	9.06
Constant temperature, impermeable	Constant flux, impermeable	0.6	200	≈ 2.6	3.1
Constant temperature, permeable	Constant flux, impermeable	0.6	200	≈ 3.1	3.21
Constant temperature, impermeable	Constant flux, impermeable	0.6	3000	NA*	7.98
Constant temperature, permeable	Constant flux, impermeable	0.6	3000	NA	13.85
Constant temperature, permeable	Constant flux, impermeable	1.0	40	≈ 1.4	1.44
Constant temperature, impermeable	Constant flux, impermeable	1.0	100	≈ 1.9	2.86

*Not available

ability of the medium to transfer heat has been doubled. When the boundary conditions are fixed temperatures, the result is a doubling of the average heat flux. When one of the boundaries is a fixed flux boundary, then the average temperature difference necessary to maintain a given heat flux is halved. Figure 3 shows some of the results to date, both experimental and theoretical, for heat transfer between isothermal, impermeable boundaries.

Experimental results for other boundary conditions were not obtained. Ribando (1977) investigated numerically the effects of a permeable top and of a constant flux bottom upon heat transfer in porous media (Table 2). In general, his results indicate that for a given Rayleigh number a permeable top increases the intensity of convection, while a constant flux bottom decreases it, compared to isothermal, impermeable boundaries. It is apparent that the correct choice of boundary conditions is very important, yet doing so is often difficult, especially since constant flux and isothermal boundaries are identical at subcritical Rayleigh numbers.

Layering and slope effects

The effects of layering and slope are of great importance to this study, since snow covers are frequently heterogeneous and are often found on hillsides. Most of the analysis of the effects of layering has been done using numerical solutions of the governing differential equations. Both the onset of convection (McKibben and O'Sullivan 1980, Richard and Gounot 1981) and heat transfer in layered porous media (Rana et al. 1979, McKibben and O'Sullivan 1981, Richard and Gounot 1981) have been treated. Some of the results have been compared favorably with experiments (Richard and Gounot 1981) and with data from geothermal reservoirs (Rana et al. 1979).

Because of the infinite number of possibilities for combinations of layers, generalized correlations are not available to predict the effects of layers on the onset of convection and heat transfer by convection. McKibben and O'Sullivan (1980) conclude that unless permeability differences between layers are 50% or more, the onset of convection is not affected. Also, when an upper layer of low permeability exists, a closed or open upper boundary does not affect the results.

The outstanding feature that distinguishes the situation in a sloped layer from that in a horizontal layer is that on a slope there will be some motion of air for any finite ΔT. At subcritical Rayleigh numbers, the flow is a simple unicellular pattern, rising along the lower warm boundary and returning downward below the cold upper boundary. In a slope of infinite extent, flow perpendicular to the slope is negligible, and thus neither the temperature profile nor the heat trans-

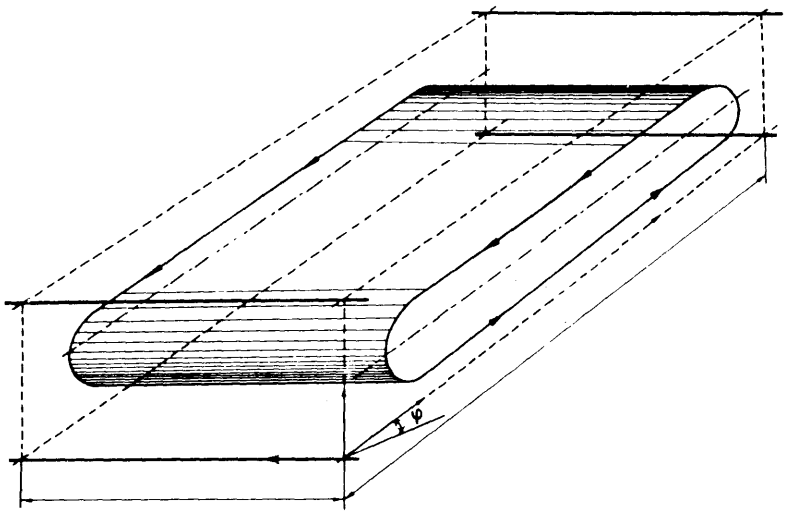

Figure 4. Unicellular convection in a sloped porous layer (after Combarnous and Bories 1975).

fer is affected. This convection is illustrated in Figure 4; the velocity profile can be described by (Bories and Combarnous 1973)

$$u(z) = \rho_o \beta g \Delta T K \sin\phi\left(\frac{1}{2} - \frac{z}{H}\right). \tag{7}$$

Thus the intensity of convection increases with increasing slope.

As the Rayleigh number increases to the critical value, the structure of convection becomes more complex. For slightly inclined slopes ($\phi < 10$-15°), hexagonal cells have been observed by Bories and Combarnous (1973). Kaneko et al. (1972) have observed transverse rolls (axis parallel to the contour) at similar low angles. The reason they observed rolls and not hexagonal cells was that the dimensions of their box were much smaller along the roll axis, and thus two dimensional convection was forced.

In more steeply inclined layers at high Rayleigh numbers, Bories and Combarnous found longitudinal rolls (axis parallel to fall line). Kaneko et al. observed a single unicellular pattern in steep layers. The two sets of observations are consistent when respective container geometries are considered. Krantz et al. (1983) observed a similar transition in field studies of patterned ground. The transition they observed takes place between 3° and 7°.

The behavior of these cells (or rolls) is similar to that in horizontal systems, except that the governing parameter, Ra, is replaced by Ra $\cos\phi$. The experimental data of Bories and Combarnous (1973) show that if the Nusselt number is plotted as a function of Ra $\cos\phi$, the result is identical to Figure 3, especially at high Rayleigh numbers. Weber (1975) extends the analytical results of Palm et al. (1972) by simply replacing g by $g\cos\phi$ in the definition of Rayleigh number. The analytical results agree well with the experimental data of Bories and Combarnous.

No work has been done on the influence of different boundary conditions or the effects of lateral confinement on convection in sloped layers. Also, the existence of the longitudinal rolls described by Bories and Combarnous (1973), superimposed on the basic uphill-downhill unicellular flow, must be better understood. No return path for the fluid is described and thus the spiral coil may not exist.

Studies of convection through snow

To date, only Akitaya (1974) and Palm and Tveitereid (1979) have studied thermal convection in snow. Akitaya's work was primarily experimental, while that of Palm and Tveitereid was entirely theoretical.

Akitaya attempted to generate convection in a layer of snow 15 cm deep, but was largely unsuccessful. He was able to generate convection only in artificial snow with an average grain size of 15 mm. That he was able to generate convection in only snow of extreme permeability is not surprising, since convection is less likely in shallow snow layers. His results with artificial snow *are* surprising because they show a step change in the effective thermal conductivity with increasing temperature gradient, rather than the continuous increase we would expect.

Akitaya's comparison of experiment with theory led him to conclude that in snow, convection occurs at a much higher than predicted critical gradient. His conclusion is not valid, however, because he used ρC_p for snow rather than for air when he calculated the conditions for the onset of convection. When correctly calculated, it is obvious why there was no convection in his natural snow experiments.

Palm and Tveitereid (1979) calculated the critical conditions for convection in snow in a similar manner to that used for other porous media. In general, their conclusion was that convection could occur only in old, coarse-grained snow subjected to severe gradients. While it is true that these are conditions under which convection is most likely, they probably underestimate the likelihood of convection under less severe situations. In particular, they used a value of air permeability for "coarse-grained" snow that is similar to that observed by Shimizu (1970) for "fine-grained" snow. Shimizu reported values about twice as large for what he calls coarse-grained snow, and Bader (1939) observed permeabilities for depth hoar as much as five times the largest considered by Palm and Tveitereid.

The theory developed in the sections above is not sufficient to fully describe convection in snow. Phase change from the net condensation or sublimation of water vapor is an important part of the heat transfer process. This was recognized by Palm and Tveitereid, but was incorporated into their analysis only insofar as the value of κ was affected in the Rayleigh number. Since their value of k_m was arbitrarily chosen, their consideration of phase change was physically meaningless. It is necessary to treat phase change as a part of the governing equations, since its influence depends on local temperatures, temperature gradients and velocities.

The boundary conditions in snow frequently include a permeable top and a constant heat flux bottom. While the influence of these boundary conditions on the onset of convection is well understood (see Table 1), their influence on the intensity of convection at Rayleigh numbers greater than critical has not been quantified. This is one of the aims of later sections of this report.

Those recently working on convection in snow have ignored the convection phenomenon associated with sloped layers. Neher (1939) recognized that flow of air occurs up a snow slope when a temperature gradient is applied, but none of his successors have made mention of this fact. He attributes the existence of thicker depth hoar layers in the upslope parts of inclined snow covers to this phenomenon. This observation would seem of vital importance in avalanche predictions because these upslope regions are frequently starting zones for avalanches.

In the following section, we address the above-stated gaps in our current knowledge. Later our findings are applied to two real problems of convection in a snow layer: First, does it occur? And second, is it important in snow metamorphism?

MODELING

A numerical model is developed here to simulate convection in a porous medium. Two forms of the model are developed, one form without phase change, which is similar to the porous media model of Ribando (1977). The second form more closely models convection through snow by

accounting for latent heat effects from vapor transport. Both models assume that the medium is isotropic and homogeneous. Boundary conditions, aspect ratio of the medium, Rayleigh number and slope may all be varied for both models. In addition, for the second model the effective vapor diffusivity (D_{eff}) and thermal conductivity (k_m) may also be varied.

In this section, the governing equations are developed and the numerical methods are outlined; in the next section the results are presented.

Equation of motion

It is assumed here that air flow through snow can be described by the empirical relation developed by Darcy. This is valid for Reynolds numbers (Re) less than a critical number for the onset of turbulent flow, which falls between 1.0 and 10.0 (Dullien 1979). The Reynolds number is defined as

$$\mathrm{Re} = \frac{\rho_f v d}{\mu_f}$$

where d is a particle diameter. Our calculations (see *Applications to Snow Metamorphism* section) reveal that a typical velocity is 0.04 cm/s. Thus for a 1-mm particle, the Reynolds number is about 0.03, and Darcy's Law should be valid.

Darcy's Law is traditionally (Scheidegger 1974) written as

$$\vec{\nabla}' p - \frac{\mu}{K} \vec{v}' - \rho_f \vec{g} = 0 \qquad (8)$$

where g is the gravitational vector and is in the same direction as the positive z axis. The velocity is averaged over a cross-sectional area that is an order larger than the pore size scale, thus the velocity is equivalent to a volumetric flux. When the fluid is made up of several components, a mass average velocity is used, defined as

$$v = \frac{\sum_i (\rho v)_i}{\sum \rho_i}$$

where the summation is over all fluid components and each v_i is the volumetric flux of the component. The primes indicate quantities later made dimensionless.

We limit ourselves to two-dimensional modeling and define the coordinate system in two dimensions as shown in Figure 5. The gravity vector has negative z and x components and thus the final term of eq 8 has the opposite sign. Introducing

$$v' = v \frac{\kappa}{H}$$

and

$$\nabla' = \frac{\nabla}{H}$$

we rewrite eq 8 as

$$\vec{v} = -\frac{K}{\mu\kappa} \nabla p + \frac{KH}{\mu\kappa} \rho_f \vec{g}. \qquad (9)$$

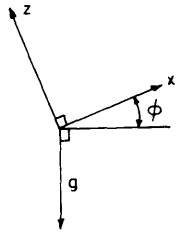

Figure 5. Two-dimensional coordinate system.

If we take the curl (∇x) of both sides, the pressure term is identically zero and the result is

$$\frac{\partial w}{\partial x} - \frac{\partial u}{\partial z} = \frac{KH}{\mu\kappa}(\vec{\nabla} x\, \rho_f \vec{g})$$

where w and u are the dimensionless velocity components in the z and x directions respectively.

To a good approximation, the density of air is a linear function of temperature over the temperature range of interest, thus we can write an equation of state of the form

$$\rho_f = \rho_o\,[1 - \beta(T' - T_o)]. \tag{10}$$

By introducing a dimensionless temperature defined as

$$T = \frac{T' - T_o}{\Delta T} \tag{11}$$

and substituting this into the density term, the equation of motion becomes

$$\frac{\partial w}{\partial x} - \frac{\partial u}{\partial z} = \frac{\rho_o KH\beta\Delta T}{\mu\kappa}(\vec{\nabla} x\, \vec{g} T)\,. \tag{12}$$

Finally, a stream function of the form

$$\frac{\partial \psi}{\partial x} = w \qquad \frac{\partial \psi}{\partial z} = -u \tag{13}$$

is introduced. The final form of the equation of motion is then

$$\nabla^2 \psi = \mathrm{Ra}\,[\cos\phi \frac{\partial T}{\partial x} - \sin\phi \frac{\partial T}{\partial z}] \tag{14}$$

where

$$\mathrm{Ra} = \frac{\rho_o g\beta\Delta TKH}{\mu\kappa} \tag{15}$$

As discussed earlier, the parameter ΔT is defined by the boundary conditions.

Energy equation

For a multicomponent system, the energy equation can be written as

$$\sum_i \frac{\partial}{\partial t}(\rho U)_i + \sum_i \nabla \cdot (\rho \vec{v} U)_i = -\nabla \cdot q - \nabla \cdot p\vec{v} + \rho_f(\vec{v} \cdot \vec{g}) - \nabla \cdot (\bar{\bar{\tau}} \cdot \vec{v}) \tag{16}$$

where the summation is over all components. Here primes are not used, although the variables are later made nondimensional. This is essentially a multicomponent form of an equation presented by Bird et al. (1960). All of the work terms have been written for a single-component fluid, because for the snow-air system the fluid is dominantly air. Kinetic energy terms have been neglected. The last term on the right side represents viscous work ascribable to energy dissipation in the fluid but, since dissipation is dominated by fluid shear at the solid matrix, we neglect this

term. The gravitation term is estimated to be four orders of magnitude less than the comparable convection term, and thus is also neglected.

Since

$$u_i = h_i - (p/\rho)_i$$

we can write eq 16 as

$$\sum_i \frac{\partial}{\partial t}(\rho h - p)_i + \sum_i [\vec{\nabla}\cdot(\rho h \vec{v}) - \vec{\nabla}\cdot p\vec{v}]_i = -\vec{\nabla}\cdot\vec{q} - \vec{\nabla}\cdot p\vec{v} \tag{17}$$

where the summation is taken over all components, which may have different velocities because they diffuse at different rates. Since

$$p_i = \rho_i / \sum_i \rho_i, \sum_i \vec{\nabla}\cdot(p\vec{v})_i = \vec{\nabla}\cdot p\vec{v} \text{ and } \sum_i \frac{\partial p_i}{\partial t} = \frac{\partial p}{\partial t}$$

the two pressure work terms are identical and cancel each other out. Rearranging, we get

$$\sum_i h_i\left(\frac{\partial \rho}{\partial t} + \vec{\nabla}\cdot\rho\vec{v}\right)_i + \sum_i\left(\rho\frac{\partial h}{\partial t} + \rho\vec{v}\cdot\vec{\nabla}h\right)_i = -\vec{\nabla}\cdot\vec{q} - \frac{\partial p}{\partial t}. \tag{18}$$

The continuity equation for each component is

$$\frac{\partial \rho_i}{\partial t} = -\vec{\nabla}\cdot(\rho_i\vec{v})_i + r_i \tag{19}$$

where r_i is the rate of production of component i. The equation of continuity for an incompressible fluid is

$$\vec{\nabla}\cdot\vec{v} = 0. \tag{20}$$

Combining eq 18 and 19 results in

$$\sum_i\left(\rho_i\frac{\partial h_i}{\partial t} + \rho_i\vec{v}\cdot\vec{\nabla}h_i + r_i h_i\right) = -\vec{\nabla}\cdot\vec{q} - \frac{\partial p}{\partial t}, \tag{21}$$

Here we deal only in the steady-state results, assuming that the phenomena in snow are at least quasi-steady, that is, changing slowly.

$$\sum_i\left(\rho_i\vec{v}\cdot\vec{\nabla}h_i + r_i h_i\right) = -\vec{\nabla}\cdot\vec{q}. \tag{22}$$

This is the general form of the energy equation we will apply.

First let us consider only air flowing through snow, with no vapor contribution (or vapor contributions independent of temperature). Then $r_i = 0$ and $v = v_a$. The resulting energy equation is then

$$\rho\vec{v}\cdot\vec{\nabla}h_a = -\vec{\nabla}\cdot\vec{q}. \tag{23}$$

We can evaluate the enthalpy by the following thermodynamic relations:

$$dh = \left(\frac{\partial h}{\partial T}\right)_p dT + \left(\frac{\partial h}{\partial p}\right)_T dP \quad , \quad \left(\frac{\partial h}{\partial T}\right)_p = C_p \quad \text{and} \quad \left(\frac{\partial h}{\partial p}\right)_T = \frac{1}{\rho}(1 - \beta T)$$

where β is the isobaric coefficient of thermal expansion. For air $\beta \approx 1/T$, and thus

$$dh = C_p dT . \tag{24}$$

Applying Fourier's law of heat conduction:

$$\vec{q} = -k_m \vec{\nabla} T \tag{25}$$

and the energy equation is, in final form,

$$(\rho C_p)_a \vec{\nabla} \cdot \vec{v} T = k_m \nabla^2 T . \tag{26}$$

This is the standard form of the energy equation used in modeling of porous media.

We now introduce vapor effects so ρ_v varies with temperature and r_i is not zero. Applying these to eq 22, along with $r_s = -r_v$, results in

$$\rho_v \vec{v}_v \cdot \vec{\nabla} h_v + \rho_a \vec{v}_a \cdot \vec{\nabla} h_a + r_v (h_v - h_s) = k_m \nabla^2 T. \tag{27}$$

At steady state $\vec{r}_v = \Delta(\rho \vec{v})_v$. Component velocities are given by

$$\vec{v}_v = \vec{v} + \vec{j}_v / \rho_v$$

$$\vec{v}_a = \vec{v} + \vec{j}_a / \rho_a .$$

The j's are the component velocities relative to the mass average velocity. Here they are considered to be caused by concentration diffusion only. Since $j_a = -j_v$, and from Fick's law of diffusion, $j_v = -D \nabla \rho_v$, we can estimate the relative contributions of diffusion to the component velocities. For an equation of state for the vapor, we use the exponential relation

$$\rho_v = \rho_o \exp[B(T' - T_o)] . \tag{28}$$

Here we have assumed that the vapor is everywhere saturated. Although this is not strictly true, typical supersaturations are usually less than 0.1% and thus have little effect on the overall diffusion process.

At 0°C, with a 0.3°C/cm temperature gradient, the diffusional flux is about 2.7×10^{-8} g/cm^2 s. The diffusional velocities are then 5×10^{-3} and 2×10^{-5} cm/s for vapor and air respectively. Since convective velocities are of the order of 0.01 cm/s, it is certainly safe to neglect at least the diffusional component of air. Also, the density of vapor is three orders of magnitude less than that of air, and since the heat capacities are similar, the second term of eq 27 is much greater than the first. The energy equation is now of the form

$$(\rho C_p)_a \nabla \cdot v T + r_v (h_v - h_s) = k_m \nabla^2 T. \tag{29}$$

From continuity for the vapor phase, $\vec{r}_v = \vec{\nabla}\cdot(\rho_v\vec{v}) + \vec{\nabla}\cdot\vec{j}_v$ at steady state, and by definition, $L = h_v - h_s$. The gradients of ρ_v as a function of temperature are obtained by differentiating the equation of state. Using these relations, and Fick's law for j_v, we find the final dimensional form of the energy equation

$$(\rho C_p)_a \ \vec{\nabla}\cdot\vec{v}\,T + L\ \vec{\nabla}\cdot\rho_v\vec{v} = k_m\nabla^2\,T + LBD\ \vec{\nabla}\cdot(\rho_v\vec{\nabla}T). \tag{30}$$

Finally, we put eq 26 and eq 30 in nondimensional form. T, ∇ and v are the dimensional quantities that are now used in nondimensional form, which is done identically to that in the *Equation of Motion* section. Then

$$\vec{\nabla}\cdot\vec{v}T = \nabla^2 T \tag{31}$$

and

$$\vec{\nabla}\cdot(T+N1)\vec{v} = \vec{\nabla}\cdot(N2\vec{\nabla}T) \tag{32}$$

where

$$N1 = \frac{L\rho_v}{(\rho C_p)_a\Delta T} \quad \text{and} \quad N2 = 1 + \frac{LDB\rho_v}{k_m}\ . \tag{33}$$

It is important to note that both $N1$ and $N2$ are functions of temperature.

Finite difference methods

Finite differences were chosen as a means of obtaining approximate solutions to the partial differential equations (PDE). The method breaks the region of interest down into discrete points, replacing the PDE with a system of algebraic equations in terms of values of the dependent variables at the discrete points. As the number of points increases, both the accuracy of the solution and the computing time increase. Finite differences are especially well suited to the present problem because of the simple geometries involved. A typical grid for the current problem is illustrated in Figure 6.

Formulas for discretizing the PDEs can be derived either from Taylor series expansions (Pinder and Gray 1977) or by integrating over control volumes around nodes. This latter method is especially useful for conservation equations such as the energy equation in the current problem. We later demonstrate this approach, which is used extensively in deriving formulae for the energy equation.

First, we will present the results for the equation of motion. Finite difference expressions, which have a truncation error of $0(h^2)$, are used for all terms; h is the spacing between grid points. The discrete form of eq 14 is

$$\frac{\psi_{i+1,j} - 2\psi_{i,i} + \psi_{i-1,j}}{h_x^2} + \frac{\psi_{i,j+1} - 2\psi_{i,j} + \psi_{i,j-1}}{h_z^2} =$$

$$\mathrm{Ra}\left[\cos\phi\left(\frac{T_{i+1,j} - T_{i-1,j}}{2h_x}\right) - \sin\phi\left(\frac{T_{i,j+1} - T_{i,j-1}}{2h_z}\right)\right]. \tag{34}$$

This form is valid at all interior nodes.

When the boundary condition is the Dirichlet condition ($\psi = 0$), we do not need to apply the PDE at the boundary

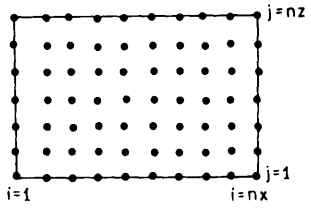

Figure 6. Typical finite difference grid.

because the value for ψ is known. However, when the top is permeable, the boundary condition is $\partial\psi/\partial z = 0$, and we must solve for ψ at the upper boundary. We cannot simply apply eq 34 because the node at index j+1 does not exist for $j = nz$. The procedure used is to employ a shadow node technique, in effect pretending that the node is there. We write a central difference form of the boundary condition as

$$\frac{\psi_{i,nz+1} - \psi_{i,nz-1}}{2h_z} = 0 \tag{35a}$$

and a backward difference form of the temperature derivative as

$$\left(\frac{\partial T}{\partial z}\right)_{j=nz} = \frac{3T_{i,nz} - 4T_{i,nz-1} + T_{i,nz-2}}{2h_z} . \tag{35b}$$

Then, by writing the PDE at j=nz, we can eliminate ψ_{nz+1} by solving for it from eq 35a. The result is an equation for ψ_{nz}:

$$\frac{(\psi_{i+1} - 2\psi_i + \psi_{i-1})_{nz}}{h_x^2} + 2\,\frac{\psi_{i,nz-1} - \psi_{i,nz}}{h_z^2} =$$

$$\mathrm{Ra}\left[\cos\phi\left(\frac{T_{i+1,nz} - T_{i-1,nz}}{2h_x}\right) - \sin\phi\left(\frac{3T_{i,nz} - 4T_{i,nz-1} + T_{i,nz-2}}{2h_z}\right)\right] . \tag{36}$$

Velocities are calculated, again using three-point central differences. For interior nodes

$$u_{i,j} = -\frac{\psi_{i,j+1} - \psi_{i,j-1}}{2h_z}$$

$$w_{i,j} = \frac{\psi_{i+1,j} - \psi_{i-1,j}}{2h_x} . \tag{37}$$

At the boundaries, the velocity component normal to the wall is zero, but the component parallel to the wall is not. The appropriate three-point backward or forward difference is then employed, similar to eq 35b.

To derive the discrete form of the energy equation, integration is performed over a control volume about each node. The discrete form may also be found from Taylor series formulas, but this method is physically less appealing and difficult to apply at the boundaries. Upwind differencing is applied to evaluate the convection terms. Essentially, this means that only nodes upstream of the control volume boundary are allowed to influence the heat transfer across the boundary. Upwind differencing is used to damp the instability associated with the non-linear, first order convective terms. The method enhances the stability of the numerical method, but at a cost in accuracy, because the upwind difference expressions have a truncation error of $0(h)$. This concept will be illustrated shortly.

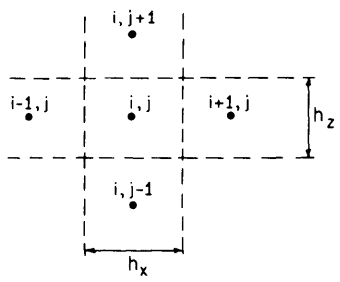

Figure 7. Control volume used for interior nodes.

The control volume used for interior nodes is illustrated in Figure 7. Earlier we derived an energy equation for single-component fluid flowing through a porous medium. The physical statement of eq 30 is that

net (conduction + convection) = accumulation.

It was assumed that the system was at steady state, so that accumulation was zero. Here we introduce a transient term so that we may numerically advance the system to its final steady state. For the control volume about the node *i,j* the accumulation over one time step Δt is written as

$$\text{acc} = (T_{i,j}^{\ell+1} - T_{i,j}^{\ell}) h_x h_z$$

where the index ℓ indicates the time step level, and T, x and z are the nondimensional variables defined earlier.

The flow of heat into the control volume by conduction in the time Δt is given by

$$\text{cond} = \left(\frac{T_{i-1,j} - T_{i,j}}{h_x} + \frac{T_{i+1,j} - T_{i,j}}{h_x} \right) h_z \Delta t + \left(\frac{T_{i,j+1} - T_{i,j}}{h_z} + \frac{T_{i,j-1} - T_{i,j}}{h_z} \right) h_x \Delta t \ .$$

Physically, the conduction terms are positive when the temperature is greater outside the control volume than inside, i.e., heat flows in. The heat flow across each boundary is simply the gradient across that boundary, which here is approximated with a central difference applied at the control volume boundary, multiplied by the area for heat transfer and the time interval.

For the convective terms, heat flows in when the fluid flows in. The heat flow attributable to convection is

$$\text{convect} = [(uT)_{i-\frac{1}{2}} - (uT)_{i+\frac{1}{2}}] h_z \Delta t - [(wT)_{j-\frac{1}{2}} - (wT)_{j+\frac{1}{2}}] h_x \Delta t$$

where u and w are positive in the positive x and z directions respectively. We define

$$u_{i-\frac{1}{2}} = \frac{u_{i-1,j} + u_{i,j}}{2} \ , \quad w_{j-\frac{1}{2}} = \frac{w_{i,j-1} + w_{i,j}}{2}$$

$$u_{i+\frac{1}{2}} = \frac{u_{i+1,j} + u_{i,j}}{2} \ , \quad w_{j+\frac{1}{2}} = \frac{w_{i,j+1} + w_{i,j}}{2} \ . \tag{38}$$

The upwind differencing concept then defines

$$T_{i-\frac{1}{2}} = \begin{cases} T_{i-1,j} & \text{for } u_{i-\frac{1}{2}} > 0 \\ T_{i,j} & \text{for } u_{i-\frac{1}{2}} < 0 \end{cases} \qquad T_{j-\frac{1}{2}} = \begin{cases} T_{i,j-1} & \text{for } w_{j-\frac{1}{2}} > 0 \\ T_{i,j} & \text{for } w_{j-\frac{1}{2}} < 0 \end{cases}$$

$$T_{i+\frac{1}{2}} = \begin{cases} T_{i+1,j} & \text{for } u_{i+\frac{1}{2}} < 0 \\ T_{i,j} & \text{for } u_{i+\frac{1}{2}} > 0 \end{cases} \qquad T_{j+\frac{1}{2}} = \begin{cases} T_{i,j} & \text{for } w_{j+\frac{1}{2}} > 0 \\ T_{i,j+1} & \text{for } w_{j+\frac{1}{2}} < 0 \ . \end{cases} \tag{39}$$

In calculating the heat fluxes across each boundary, we have assumed that the temperature and temperature gradient normal to the control volume boundary are constant along the bound-

ary. Beier et al. (1983) account for variations along the boundary and find that the second order terms are of $0(h^3)$ and $0(h^4)$ for the convective and conductive terms respectively. Thus each is less than the first order truncation error term by $0(h^2)$ and can be neglected for reasonably fine grids.

The complete energy equation is then

$$\frac{T_{i-j}^{\ell+1} - T_{i-j}^{\ell}}{\Delta t} = \frac{(T_{i+1} - 2T_i + T_{i-1})_j}{h_x^2} + \frac{(T_{j+1} - 2T_j + T_{j-1})_i}{h_z^2}$$

$$- \left(\frac{(uT)_{i+\frac{1}{2}} - (uT)_{i-\frac{1}{2}}}{h_x} \right)_j - \left(\frac{(wT)_{j+\frac{1}{2}} - (wT)_{j-\frac{1}{2}}}{h_z} \right)_i . \tag{40}$$

The terms on the right-hand side may be evaluated at either the ℓ or ℓ+1 time step level, depending on the solution scheme used. This same form can be obtained by applying central differences to the conduction terms, first order upwind differences to the convection term, and a first order forward difference to the transient term.

When the effects of phase change are considered (eq 32), the finite differences used follow the same basic concepts. Convection of vapor is treated in a similar way to the convection of air. Diffusion of vapor is treated in a manner similar to that of conduction of heat. The discrete form of eq 31 (again with a false transient) is

$$\frac{(T_{i,j}^{\ell+1} - T_{i,j}^{\ell})}{\Delta t} = \frac{N2_{i+\frac{1}{2}}(T_{i+1} - T_i) - N2_{i-\frac{1}{2}}(T_i - T_{i-1})}{h_x^2}$$

$$+ \frac{N2_{j+\frac{1}{2}}(T_{j+1} - T_j) - N2_{j-\frac{1}{2}}(T_j - T_{j-1})}{h_z^2}$$

$$- \frac{u_{i+\frac{1}{2}}(T + N1)_{i+\frac{1}{2}} - u_{i-\frac{1}{2}}(T + N1)_{i-\frac{1}{2}}}{h_x} \tag{41}$$

$$- \frac{w_{j+\frac{1}{2}}(T + N1)_{j+\frac{1}{2}} - w_{j-\frac{1}{2}}(T + N1)_{j-\frac{1}{2}}}{h_z} .$$

$(T + N1)_{i+\frac{1}{2}}$, etc., are computed using upwind differencing as with $T_{i+\frac{1}{2}}$ in eq 39. $N2_{i+\frac{1}{2}}$, etc., are defined in a manner similar to the velocities defined in eq 38, i.e., the average of the two nodes adjacent to the nodal boundary is taken. Velocities at the node boundaries are computed as in eq 38.

Applying the finite difference formulae derived from Taylor series is much more difficult at the boundaries, and thus the control volume approach proves superior there. Next we shall illustrate the approach for an adiabatic, impermeable side wall. Complete derivations for all of the cases of interest are given in Appendix A.

The control volume is defined in Figure 8.

The boundary condition is that no h[illegible]s through the wall. Thus the compo[illegible]nents of the ener[illegible]tion are

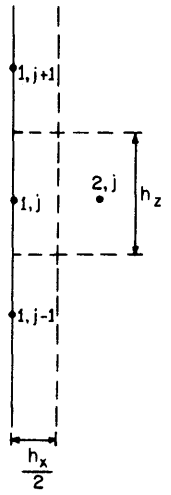

Figure 8. Control volume.

$$\text{accumulation} = (T_{1,j}^{\ell+1} - T_{1,j}^{\ell})\frac{h_x h_z}{2}$$

$$\text{conduction} = \left(\frac{T_{2,j} - T_{1,j}}{h_x}\right) h_z \Delta t + \left(\frac{T_{1,j+1} - T_{1,j}}{h_z} + \frac{T_{1,j-1} - T_{1,j}}{h_z}\right)\frac{h_z}{2}\Delta t$$

and

$$\text{convection} = -(uT)_{1+\frac{1}{2}} h_z \Delta t + [(wT)_{j-\frac{1}{2}} - (wT)_{j+\frac{1}{2}}]\frac{h_x}{2}\Delta t$$

Rearranging and combining, we find the final form to be

$$\left(\frac{T^{\ell+1} - T^{\ell}}{\Delta t}\right)_{1,j} = 2\left(\frac{T_{2,j} - T_{1,j}}{h_x^2}\right) + \frac{T_{1,j+1} - 2T_{1,j} + T_{1,j-1}}{h_z^2}$$

$$- \frac{2(uT)_{1+\frac{1}{2}}}{h_x} - \left[\frac{(wT)_{j+\frac{1}{2}} - (wT)_{j-\frac{1}{2}}}{h_z}\right]. \qquad (42)$$

While the correct form of the conduction terms could be found from a shadow node technique similar to the one employed earlier, the correct form of the convection term is much more difficult to derive.

Numerical solution

An Alternating Direction Implicit (ADI) scheme is used to evaluate the algebraic equations (Pinder and Gray 1977). The method sweeps the grid line by line, first in the x direction, then in the z direction. The scheme is implicit in that the equations written about each node are solved simultaneously for each successive line. Thus each algebraic equation contains more than one unknown. When solving the equations for a line swept in the x direction, the derivatives in x are evaluated at the time step level ℓ+1 and derivatives in z are evaluated at the time step level ℓ. The alternatives to a line-implicit scheme are to solve the equations explicitly, where new values are calculated on a node by node basis, or to solve the equations directly, in which case the values for the entire grid are calculated simultaneously. The ADI method is more stable than the explicit method, thus allowing much larger time steps to be used. The advantage over direct methods is that the matrix of coefficients is not zero only on three main diagonals, and thus the system of equations may be solved simply and efficiently without evaluating all of the zeros. An explicit form of this program was originally developed, and was found to be much slower and more costly.

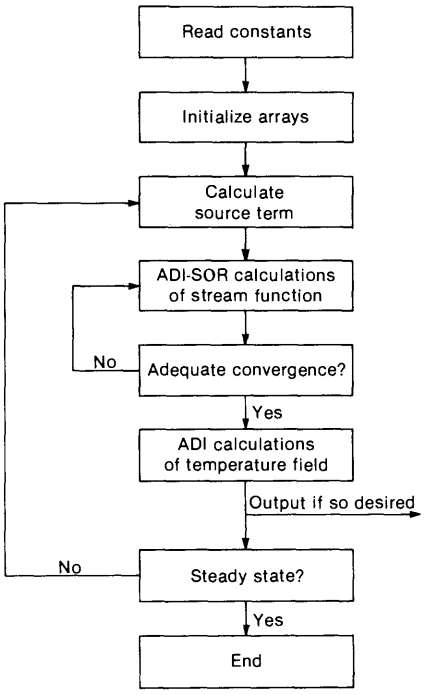

Figure 9. Flow diagram for computer codes CONVAP and CONVEC.

The computing flow chart is given in Figure 9. Two FORTRAN programs were developed: One

uses eq 33 for the energy equation, and thus accounts for latent heat, while the other uses eq 31, and does not account for latent heat effects. The codes are designated as CONVAP and CONVEC respectively. The programs differ only in the energy equation used, and thus Figure 9 applies to both codes.

The initial temperature profile varied linearly in z and was constant in the x direction. The stream function was set equal to zero over the entire grid, corresponding to a no-flow situation. A temperature perturbation was introduced prior to the first stream function calculation to start the flows. The location and magnitude of this perturbation affects the transient response but not the final steady state.

Typically, most of the computing time was used to obtain the iterative solution of the equation of motion. This equation was therefore overrelaxed (Pinder and Gray 1977) to speed convergence. In essence, what the overrelaxation does is to weight the value of $\psi_{i,j}^{\ell+1}$ to make the equation more or less implicit. It was found that an optimum value of the relaxation coefficient was 1.7, where 2.0 is fully implicit and 0.0 is fully explicit. The convergence of the solution at a time step was adequate when for all i and j

$$\frac{|\psi_{i,j}^{new} - \psi_{i,j}^{old}|}{|\psi_{max}| + |\psi_{min}| + 0.01} \leq 10^{-4}$$

where ψ_{max} and ψ_{min} are the maximum and minimum values of the stream function calculated during iteration.

Several criteria were used to determine if the solution was at a steady state. The most reliable was to monitor energy conservation. At steady state, all heat flowing in must flow out. Since the lateral boundaries are adiabatic, this implies that the heat flux at the bottom be equivalent to the heat flux at the top. In nondimensional form, the heat flux is the Nusselt number. The conservation of energy was monitored by observing the ratio $|(Nu_{top} - Nu_{bot})/Nu_{bot}|$. The equations used for calculating the Nusselt numbers at the boundaries are derived in Appendix A.

For each run, the energy balance ratio would reach a minimum value because of accuracy limitations of the solution. Better conservation (a lower minimum balance) could be achieved by refining the grid. Choice of the time step did not affect the final steady state or the energy conservation achieved. Thus the final steady state was independent of the path followed to obtain it.

Choice of the proper time step was important in the speed with which the solution converged. Too small a time step resulted in smooth but very slow convergence. Too large a time step would produce an oscillating solution that would overshoot the steady state, thus also requiring a long solution time. If the time step was much too large, the solution would not converge to a steady state. From experience we found that the optimum time step size was usually between 0.01 and 0.05. Grid spacing size did not seem to affect the choice of Δt, but the value of the Rayleigh number did. It was found to be necessary to use a smaller time step as the Rayleigh number increased.

Verification of the model

To test the model, runs were made that could be compared directly to results in the literature. Most of the results in the literature are for the basic case of convection in a horizontal layer bounded by isothermal, impermeable surfaces. Figure 3 shows some of the results for this case. Experimental results (compiled by Combarnous and Bories) are shown, along with analytical results of Palm et al. (1972) and Combarnous and Bories (1975). The simple relation deduced by Elder (1967),

$$Nu = Ra/Ra_{cr} \tag{43}$$

which is valid for $Ra/Ra_{cr} \geq 1$, is shown for comparison. We conclude that the relation of Elder describes the experimental results reasonably well. Figure 10 shows numerical results from our model for the same boundary conditions as Figure 9, and makes a favorable comparison with eq 43. The runs leading to these results were done with AR = 1, which is equivalent to the cell size at the onset of convection. Runs are made only for Rayleigh numbers just above the critical value, where the cell size is not too different from that at the onset. By comparing the results of Elder to the experimental data, we conclude that our numerical model, which agrees with eq 43, is actually a better tool for predicting heat transfer rates than either of the analytical results.

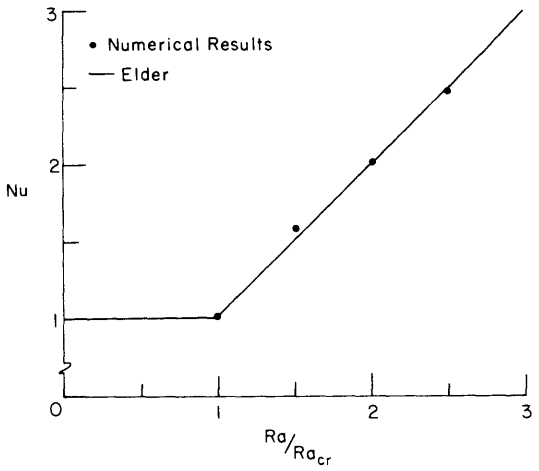

Figure 10. Numerical results and the relation deduced by Elder (1967) for convection between isothermal, impermeable boundaries.

When the bottom boundary is a constant flux thermal condition, we have only the numerical results of Ribando (1977) for comparison. Table 3 shows numerical results from our model with those of Ribando for identical conditions. Nusselt numbers for Ribando are estimated from his plots of isotherms, using the temperature difference at the midpoint of the top and bottom boundaries. Nusselt numbers for the present model are calculated by integration along the boundaries to calculate an average ΔT. Agreement for all cases is very good.

Finally, we test the model by trying to predict the onset of convection. This is done for the closed top isothermal and open top isothermal cases. Aspect ratios used are those of a single cell size at the onset of convection, calculated from the critical wavelength values given in Table 1. While it is not really practical to identify an exact onset point, it is possible to find a narrow range in which the onset point lies. The upper and lower limits indicate Rayleigh numbers at which convection clearly was and was not occurring respectively. We find that $38.0 < Ra_{cr} < 41.0$ and $26.0 < Ra_{cr} < 28.0$ for the closed and open top cases respectively. The corresponding analytical results of Ra = 39.5 and Ra = 27.1 fit within the observed range for each case.

The effects of phase change have yet to be dealt with in the literature, and thus no means of testing the model for significant phase change exist. Experimental and theoretical results exist for convection in a sloped layer, and the model predicts the general trends indicated by the pub-

Table 3. Comparison of published values with this study. All values are based on numerical calculations. Nusselt numbers for the results of Ribando are estimated from plots of isotherms. (After Ribando [1977] and Klever [1983].)

Boundary conditions	*AR*	*Ra*	*Nu*	Ψ_{max}	*Source*
Open top, constant	1.0	40	≈1.4	1.44	Ribando
flux bottom	1.0	40	1.411	1.44	Present work
Closed top, constant	1.0	100	≈1.9	2.86	Ribando
flux bottom	1.0	100	1.951	2.82	Present work
Closed top,	0.6	200	4.07	6.87	Ribando
isothermal bottom	0.6	200	NA	6.74	Klever
	0.6	200	4.02	6.69	Present work

lished works. However, the manner of presentation of results in the literature obscures some of the physical phenomena that occur in sloped layers. We have shown here that the model is a reliable tool for analyzing convection in horizontal porous media and it should allow us to study cases for which little data are currently available.

MODELING RESULTS

The effects of boundary conditions on heat transfer and air velocity are studied using the model. Subsequently, the effects on heat transfer attributable to latent heat release by phase change are analyzed and found to be a function of the diffusivity. Finally, we use the model to investigate several issues of importance in sloped layers, including the effects of lateral confinement.

Effects of constant flux and permeable boundaries on convection in horizontal layers

The work of Ribando (1977) is an important starting point in the discussion of the effects of boundary conditions upon convection in horizontal layers. He developed the mathematical forms of the boundary conditions of interest, and applied them to several simple cases. The aim here is to more thoroughly investigate the effects of these boundary conditions, so that the more general conclusions about the effects on heat transfer can be made.

Figure 11 shows the steady-state results of runs for $Ra/Ra_{cr} = 1.5$ for four combinations of boundary conditions. The aspect ratio in each case corresponds to the size of a single cell at the onset of convection, for the given boundary conditions. When the Rayleigh number is greater than the critical value, the size of a convec-

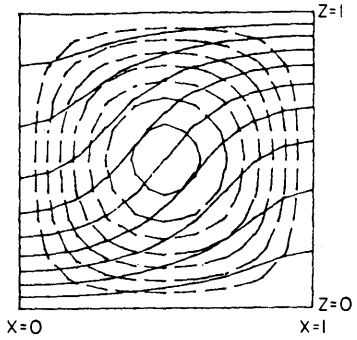

a. Closed top, isothermal bottom.

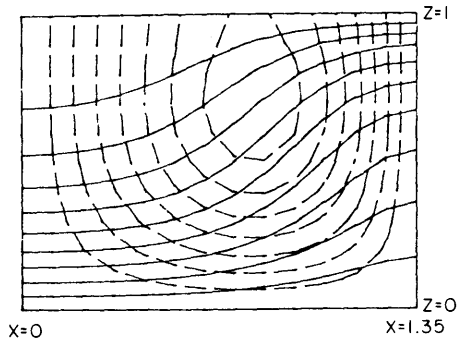

b. Open top, isothermal bottom.

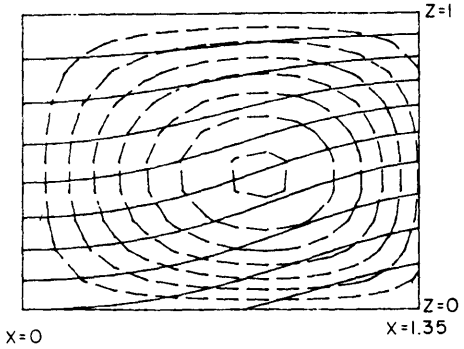

c. Closed top, flux bottom.

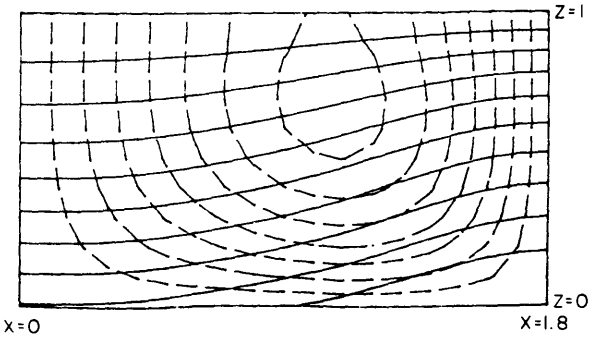

d. Open top, flux bottom.

Figure 11. Isotherms (solid lines) and streamlines (dashed lines) for $Ra/Ra_{cr} = 1.5$ for boundary conditions as labeled.

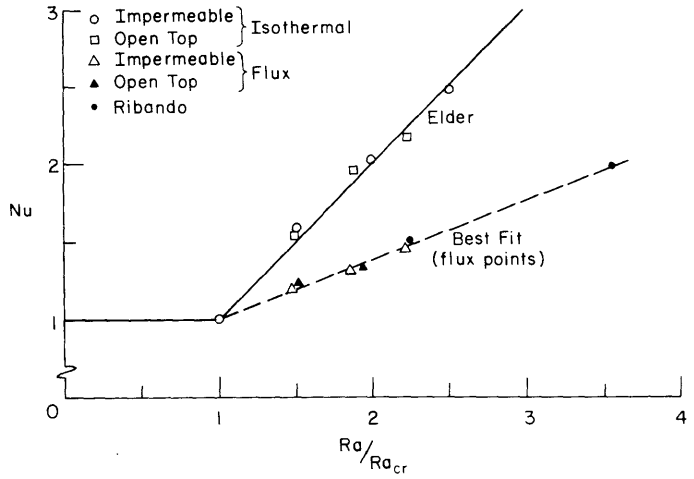

Figure 12. Heat transfer results of the numerical modeling in this report, and some results of Elder (1967) and Ribando (1977).

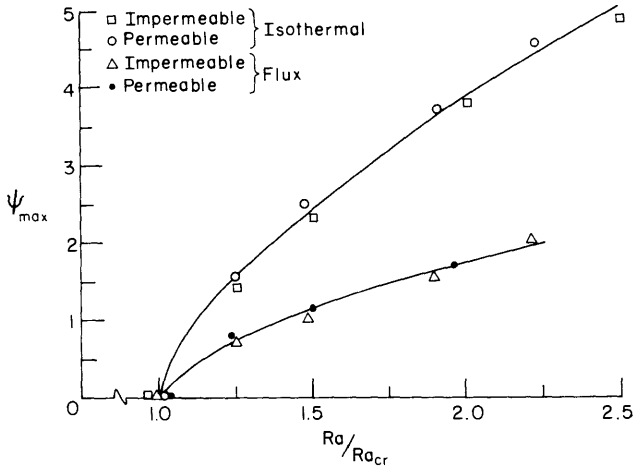

Figure 13. Maximum value of the stream function versus Ra/Ra_{cr} from the numerical results of this report.

tion cell is smaller than that at the onset, which explains the asymmetrical behavior observed in Figure 11.

Figure 12 shows the Nusselt number versus Ra/Ra_{cr} for each of the same combinations of boundary conditions. A key conclusion from the present results is that simple relations for heat transfer as a function of Ra/Ra_{cr} depend only on the bottom thermal boundary condition. For an isothermal bottom, Elder's equation (eq 43) works well.

When the bottom is a constant flux thermal boundary condition, we propose

$$Nu = 1 + 0.365\left(\frac{Ra}{Ra_{cr}} - 1\right) \tag{44}$$

as a simple model of heat transfer. Ribando's results for the constant flux case are also presented in Figure 12, for comparison. His results agree well with eq 44, although he used an aspect ratio of 1.0 for each run. The actual aspect ratio above the onset of convection is not known with certainty, but we do know that it is smaller than that on the onset of convection. Thus, at least, the geometry used by Ribando moves us in the correct direction in approaching the optimal cell size. Similar results are found with different geometries, so it appears that the aspect ratio is of little importance, as long as the aspect ratio used is near that at which heat transfer is maximized.

Figures 13 and 14 show ψ_{max} and w_{max}, respectively, again as functions of Ra/Ra_{cr}. We note that again the relations are dominated by the lower thermal boundary condition. The up-

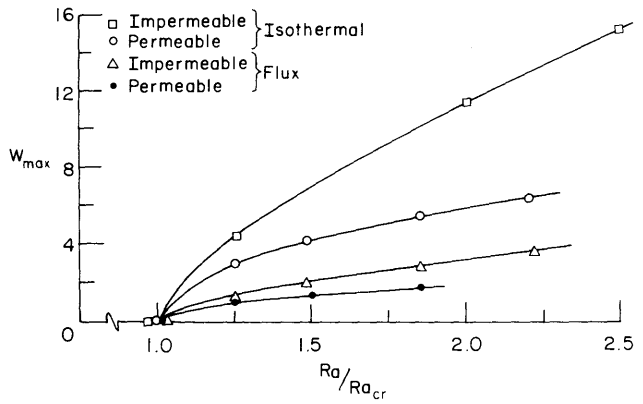

Figure 14. Maximum vertical velocity versus Ra/Ra_{cr} from the numerical results of this report.

per permeability boundary condition is more important in determining the maximum velocity, probably because the aspect ratios change with the upper boundary condition. If ψ_{max} is similar, $\partial\psi/\partial x$ will decrease as the aspect ratio increases. Thus it is expected that, for a given Ra/Ra_{cr}, the maximum velocity would be less for an open top layer. The values of velocity are important in our discussions of the effects of convection on snow metamorphism.

Effects of phase change on convection

Comparing eq 26 and 29, we find that the effect of vapor transport per se arises from the net rate of phase change between solid and fluid. Henceforth, we refer to vapor transport effects as phase change effects, since only with phase change is there an effect on the energy equation. As shown in eq 29, phase change comes about as a result of the divergence of the vapor flux. There are two contributions to the vapor flux, diffusive and convective. Earlier we discussed the effects of diffusive vapor transport through snow, and found some uncertainty in the value of D_{eff} primarily because of uncertainty over the role of interparticle vapor flow. Thus, we will vary D_{eff} to examine what effects its magnitude might have.

Earlier we defined the Rayleigh number (eq 5) as

$$\mathrm{Ra} = \frac{\rho_o \beta g \Delta T H K}{\mu \kappa}$$

where κ was defined as $k_m/(\rho C_p)_f$. In our derivation of the equation of motion, κ was introduced as a scaling factor, and could conceivably have several definitions. However, the energy equation is greatly simplified when κ is defined as above. For a single-component fluid flowing through a porous medium, the medium's thermal conductivity is assumed to be constant throughout. For snow, we have an effective thermal conductivity that strongly depends on temperature, and thus is not suitable for use as a scaling factor. Thus we will use k_m, which is the thermal conductivity ascribable to conduction through the ice and air, and which is essentially independent of temperature. Note that $k_m = k_{eff} - k_v$. When the temperature of the top surface is low ($T < -20^\circ$C), the vapor density is very low and thus transport of heat by the vapor is negligible, and κ used in the Rayleigh number is truly descriptive of the heat transfer process. However, near the bottom, where the temperature is higher, and vapor density higher, κ and thus the Rayleigh number do not fully describe the heat transfer process.

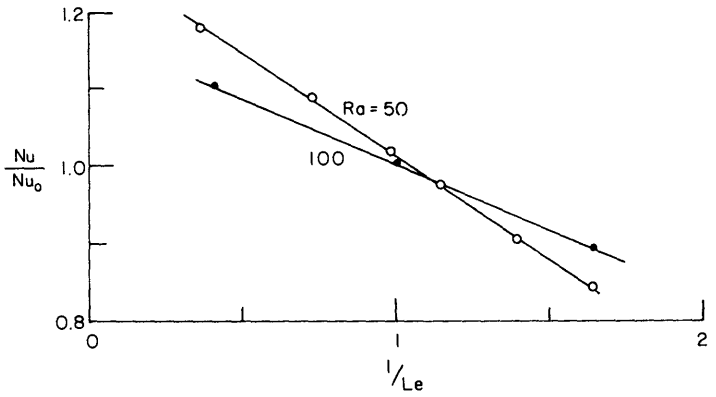

Figure 15. Ratio of heat transfer with phase change to heat transfer without phase change for two values of the Rayleigh number versus Lewis number, from numerical modeling of this report.

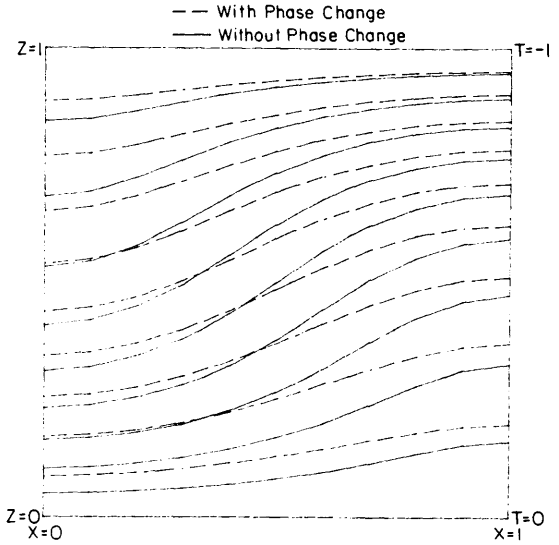

a. Le = 0.39.

Figure 16. Isotherms for convection with and without phase change (Ra = 50; isothermal, impermeable boundaries; AR = 1.0).

We can at least qualitatively analyze the effects of phase change, for a given Rayleigh number, by weighing the relative contributions of the convective and diffusive phase change terms. If convective phase change dominates, then we expect convection to be more intense than analysis with a single-component fluid would lead us to believe, and vice versa. We rewrite eq 31 as

$$\left[1+\frac{L\,B\rho_v}{(\rho C_p)_a}\right]\vec{\nabla}.\vec{v}T=\vec{\nabla}\cdot\left[\left(1+\frac{D_{eff}LB\rho_v}{k_m}\right)\vec{\nabla}\ T\right]. \tag{45}$$

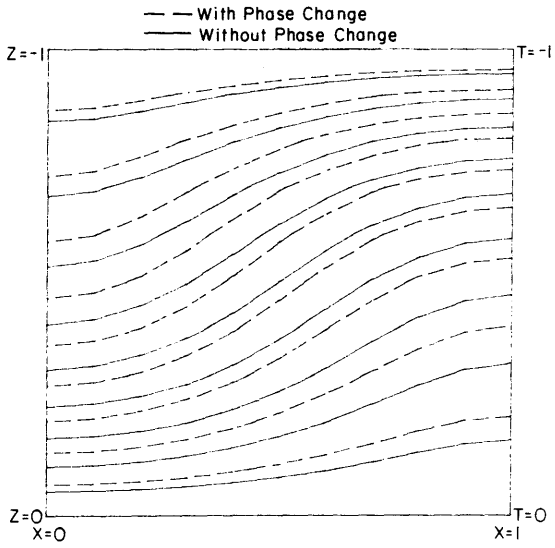

b. Le = 1.0.

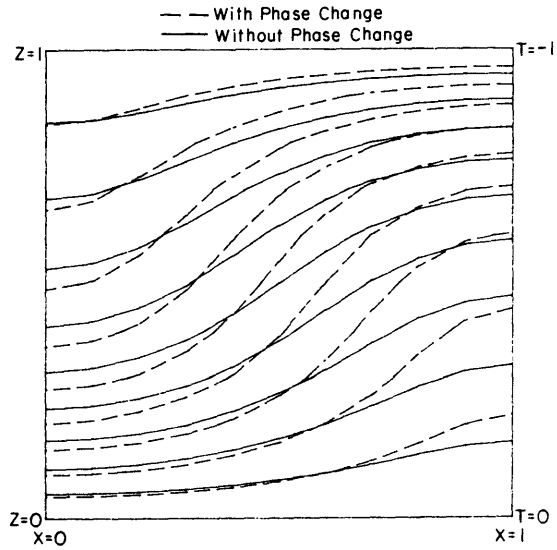

c. Le = 1.36.

Figure 16 (cont'd).

If the dimensionless parameter in the convection term is greater than the parameter in the conduction term, we expect convection to be intensified. This is true if D_{eff}/κ is less than 1.0. κ/D_{eff} is the Lewis number. If the Lewis number is less than 1.0, convection is damped, and if it is greater than 1.0, it is intensified. Figure 15 shows numerical results for various values of the Lewis number. The ordinate is the ratio of heat transfer with phase change to heat transfer without phase change. The model results closely follow the expected result that near Le = 1.0, phase change has little effect on heat transfer. However, for even small deviations from Le = 1.0, phase change has significant effects on heat transfer. The range of Lewis numbers that the numerical results cover gives approximate upper and lower limits for low density, dry snow.

Figure 16 shows the effects of Lewis number on the temperature distribution at steady state. The relative amounts of distortion from a linear temperature profile are more important than the

exact positions of the isotherms. When the Lewis number is less than 1.0, the isotherms are less distorted than the case with no phase change, and when the Lewis number is greater than 1.0, the isotherms are more distorted. For Le = 1.0, the isotherms are of similar shape. The offset between isotherms is a result of the diffusive term changing the temperature profile in the absence of convection.

Convection in sloped layers

In the *Layering and Slope Effects* section, the topic of convection in sloped layers was introduced and it was noted that some confusion existed in the literature over the effects of slope. The aim here is first to clarify the role of lateral confinement on convection in a sloped layer, and then to quantify the effects of an open top on convection in a sloped layer. All discussions in this section ignore the effects of phase change and isolate the role of slope.

The modeling efforts here are directly comparable to the experiments of Kaneko et al. (1974). Their experiments were done in a narrow slot of AR = 3.0, which allowed only two-dimensional convection. Their basic conclusion was that the Nusselt number could be represented by the relation

$$Nu = 0.082(Ra \cos\phi)^{0.76} \tag{46}$$

for $10 < \phi < 30$ degrees and $Ra \cos(\phi) > 40$. Our numerical results indicate that this is an approximate representation of heat transfer but it obscures some of the behavior of convection in an inclined porous medium. Figure 17 shows the results of Kaneko et al. (1974), and the present numerical results as a function of $Ra \cos(\phi)$. For a given slope, the Nusselt number increases in a fashion similar to that described by eq 46, but for a given Rayleigh number, heat transfer either increases or decreases with increasing slope.

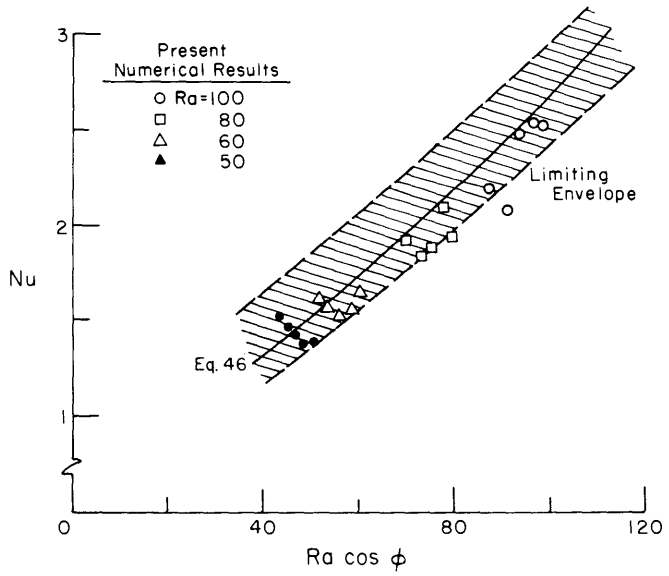

Figure 17. Nusselt number as a function of Ra cosϕ from this report's numerical results and the experimental results of Kaneko et al. (1974). The envelope represents the extent of experimental scatter in the work of Kaneko. Both our computations and the experiments of Kaneko are done for AR = 3.0.

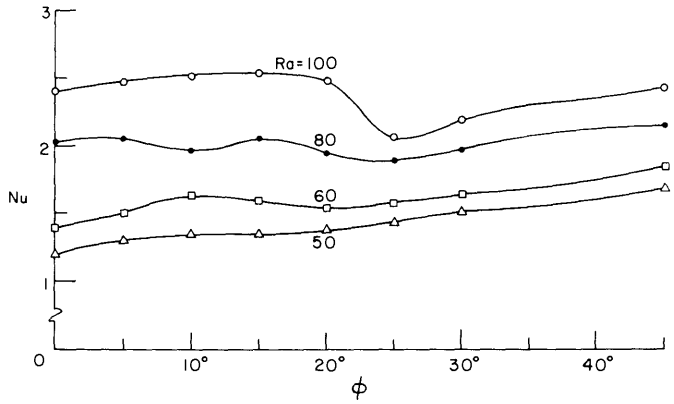

Figure 18. Nusselt number from the present numerical results versus angle of inclination. Computations done on a grid of aspect ratio equal to 3.0, with isothermal, impermeable boundaries.

Figure 18 shows the Nusselt number versus slope for various values of the Rayleigh number. The changing gradient of these curves can be explained in terms of the two competing forms of convection that are at work. We describe them in terms of the analogous convection in a fluid layer, the best known of which is the classic Benard convection in a horizontal layer with cold top and hot bottom. Convection is multicellular above a critical value of the Rayleigh number and increases in intensity as the Rayleigh number increases. The second form, or Rayleigh convection, refers to flows driven by lateral temperature differences. Convection then occurs for any value of the Rayleigh number and increases in intensity as the Rayleigh number increases. It is Rayleigh convection that drives the simple unicellular flow described by eq 7. From eq 7 we can see that the intensity increases with ϕ.

One of the assumptions leading to the derivation of eq 7 is that the temperature profile remains linear, or analogously, that heat transfer normal to the flow is not affected. This is strictly true only in the limit as the layer length becomes large. In a laterally confined layer, flow is curved by end effects, and thus a mechanism for heat transfer between hot and cold exists. The intensity of this heat transfer process must increase as the angle increases because the velocities increase.

Weber (1975) analytically treats the case of convection in an infinite layer, and finds that heat transfer is indeed a function of Ra cosϕ. In this case, Benard convection is the only heat transfer mechanism, and thus the driving force for Benard convection must decrease as the angle increases.

Referring back to Figure 18, we see that generally the Nusselt number first increases with increasing slope, then decreases, and then increases again. This happens because the interaction between Rayleigh and Benard convection results in a changing cell pattern. While the heat transfer because of Rayleigh convection increases continuously with increasing slope, the heat transfer because of Benard convection decreases substantially when the number of convective cells decreases. For a Rayleigh number of 100.0, the number of cells decreases from three cells at a slope of 15° to one cell at a slope of 25°. The heat transfer and the Nusselt number decrease accordingly. At the intermediate value of 20° there are still three cells but the middle cell is very weak and does not contribute much to the heat transfer. Accordingly, the Nusselt number is less at 20° than at 15°, but the big decrease occurs at 25° because only one cell is active. This leads to the conclusion that while Benard convection is a more powerful heat transfer mechanism, Rayleigh convection also contributes to heat transfer when the layer is confined. Rayleigh convection is especially important at Rayleigh numbers near Ra_{cr}, where Benard convection is weaker.

If there is no transition from multicellular to unicellular convection, no drop in heat transfer is expected at slopes up to 45°. Figure 19 shows the results of runs done with an aspect ratio of

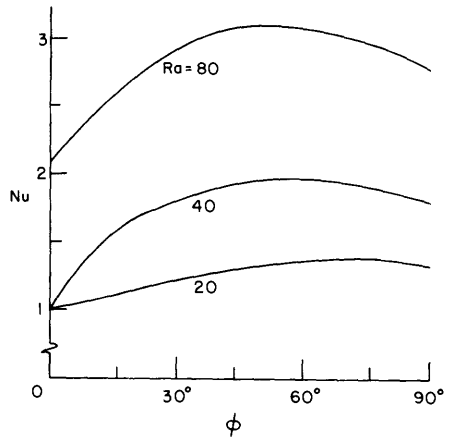

Figure 19. Nusselt number from the present numerical results versus angle of inclination. Computations done on a grid of AR = 1.0, with isothermal, impermeable boundaries.

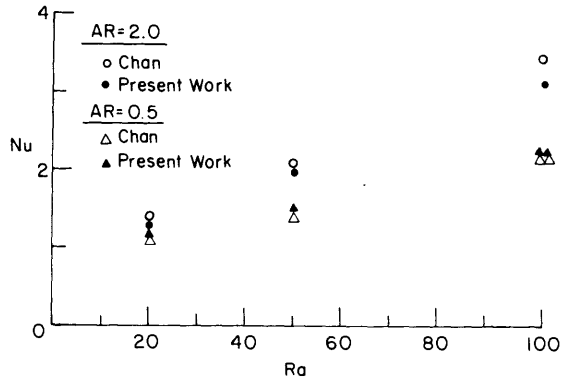

Figure 20. Nusselt number versus Rayleigh number for two different aspect ratios of an angle of inclination of 90°. Our numerical results are compared with those of Chan et al. (1970).

1.0, where unicellular convection is forced on the system. No transition in the range of 10°-30° is observed, but a decrease in heat transfer at large ($\phi > 60°$) angles is observed. This is because the driving force for convection can be thought of as the sum of the Benard and Rayleigh contributions and is thus proportional to $\cos\phi + \sin\phi$. This quantity is a maximum at 45°, and we can see that at the larger Rayleigh numbers, this is about where the maximum occurs. At lower Rayleigh numbers, Benard convection is not so important in the heat transfer process, and thus the maximum is shifted. As shown in Figure 20, our results agree well with those in the literature for $\phi = 90°$.

Secondary shifts occur in Figure 18 at 5° and 10° for Rayleigh numbers of 60.0 and 80.0 respectively. These small dips take place when the layer is in the process of shifting cell forms. In each case one smaller cell formed in the middle of two larger ones. Although the solution did converge, this cell form would seem to be unstable, and is probably an inefficient convective pattern for transferring heat.

We now turn to the important issue of convection in a sloped layer of snow, where lateral confinement is less likely to be important. If the snow layer is homogeneous, but has an impermeable

crust on its surface, convection at subcritical Rayleigh numbers is described by eq 7. If impermeable layers are present internally in the snow, eq 7 describes the convection between the layers, with the Rayleigh number based on the properties and boundary conditions of the internal layer.

Frequently, the top of the snow layer is open to the air, and the boundary condition is one of no flow in the x direction (Ribando 1977). By following Combarnous and Bories' (1975) derivation of eq 7, we can derive a similar expression for subcritical flow in a layer with an open top. Assuming that the layer is of infinite length, $w = 0$ and $dw/dz = 0$,

$$T = T_{bot} - (T_{bot} - T_{top})\frac{z}{H} \tag{47}$$

where T_{top} and T_{bot} refer to the temperature of the isothermal boundaries. For an incompressible fluid, the equation of continuity is then

$$\frac{\partial u}{\partial x} = 0 . \tag{48}$$

The one-dimensional form of Darcy's law is

$$u(z) = -\frac{K}{\mu}\frac{\partial p}{\partial x} - \frac{K}{\mu}\rho_o g(\sin\phi)[1-\beta(T-T_o)] . \tag{49}$$

Taking the derivative with respect to z, we have

$$\frac{\partial u}{\partial z} = -\frac{K}{\mu}\frac{\partial^2 p}{\partial z \partial x} + \frac{K}{\mu}\rho_o g(\sin\phi)\frac{\partial T}{\partial z} . \tag{50}$$

This is simplified for our case because $\partial p/\partial z \approx 0$ and $\partial T/\partial z \approx -\Delta T/H$, where ΔT is $T_{bot} - T_{top}$. Integrating with respect to z, and applying $u(H) = 0$, we get

$$u(z) = -\frac{K}{\mu}\rho_o g \beta(\sin\phi)\frac{\Delta T}{H}(z-H). \tag{51}$$

Introducing the scaling factors κ/H and H for velocity and distance, respectively, we redefine u and z so that the nondimensional result is

$$u(z) = \mathrm{Ra}(\sin\phi)\,(1-z). \tag{52}$$

Figure 21 shows this analytical result along with numerical results for a sloped layer of aspect ratio 6.0. The agreement is good at low angles of inclination, but deviates significantly at higher angles. This discrepancy arises because end effects are included in the numerical model but not in the analytical model.

At higher Rayleigh numbers, there may be multicellular convection in layers with an open top. Given the results of the previous section, we expect that convection in such a layer will behave in a manner similar to a layer with a closed top. Thus we expect the critical Rayleigh number for the onset of Benard convection in a layer with permeable top and isothermal bottom to be

$$\mathrm{Ra}_{cr} = \frac{\mathrm{Ra}_{cr_o}}{\cos\phi} = \frac{27.1}{\cos\phi} . \tag{53}$$

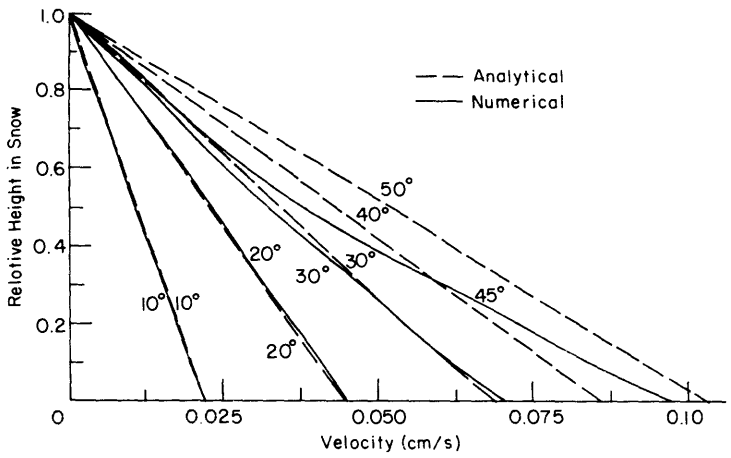

Figure 21. Velocity profiles for convection in a sloped layer with a permeable top. Analytical (eq 51) and numerical results for $K = 2.4 \times 10^{-4}$ *cm*^{2}, $\Delta T = 20°C$. *Analytical results are for an infinitely long layer, while numerical results are for AR = 6.0.*

We also expect heat transfer results to follow the same patterns as in a closed layer, with Benard convection dominating in infinite layers and both Rayleigh and Benard convection influencing heat transfer in confined layers.

A numerical model has been developed and utilized to describe thermal convection in snow. In particular, the influences of constant flux bottom and permeable top boundary conditions, of phase change and of inclination of the snow cover have been described and quantified. Each is found to have a significant effect on both the intensity and frequency of convection. The important topic of layering has not been discussed here, but has been dealt with in the literature and is well understood. In the following sections, we discuss experiments performed in an effort to further test our numerical model, and then apply the findings of this section in discussing the importance of convection in snow covers.

EXPERIMENTS

Introduction

We now experiment with convection through a horizontal porous layer that is confined, with a warm bottom and cool top. Similar experiments have frequently been done by others working with porous media, but some significant differences exist. Here the lower thermal boundary condition is a constant flux, rather than a constant temperature boundary as has been used previously. In addition, when snow is used, phase change effects are an important component of the heat transfer.

We will describe the apparatus used, the data acquisition equipment and the data analysis. The experimental results are presented in the next section and we compare these results with relevant numerical and theoretical results.

Experimental apparatus

Experiments were done using glass beads with air as the fluid, glass beads with water and dry snow with air. The apparatus used in the glass bead experiments was substantially different from that used in the snow experiments, but the data collection system was essentially the same.

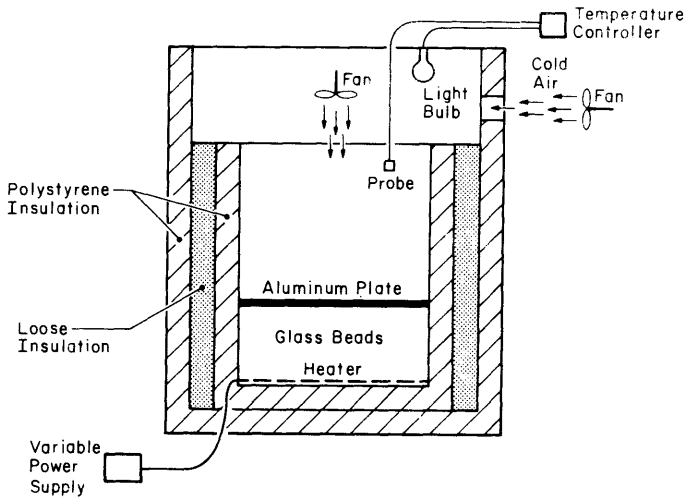

Figure 22. Apparatus for glass bead experiments.

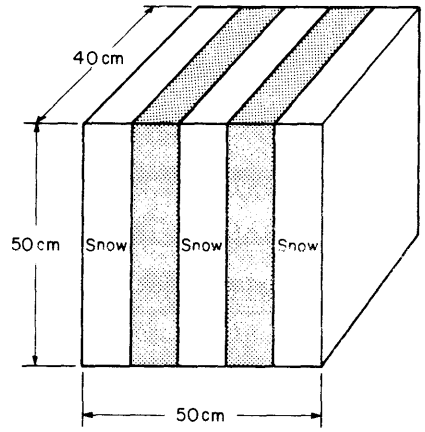

a. Snow samples separated by insulation.

Figure 23. Apparatus for snow experiments.

Experiments were first performed on glass beads to gain experience in doing experiments on natural convection before moving to the more difficult and unknown problems of convection in snow. Figure 22 shows the apparatus used for the glass bead experiments. At the top boundary cold air was blown over an aluminum plate; the air temperature was kept constant by using a heater, connected to a temperature controller. At the bottom boundary, electric heat pads were used to supply the constant heat flux. The flux rate was controlled by regulating the voltage input using a variable power supply. The glass bead layer was approximately 40 by 40 cm by 15 cm deep. When water was the saturating fluid, a plastic liner was used to retain it.

Figure 23a shows a three-dimensional view of the snow experiment, while Figures 23b and c are schematics of the experiment. Because of the low thermal conductivity of snow, heat losses out the sides would have been unacceptably large if the same apparatus was used for both glass beads and snow. A guarded technique similar to that of Buretta and Berman (1976) was used with a tall, narrow snow sample (50 by 40 cm by 10 cm high) surrounded by polystyrene insulation. The large sides (i.e., front and back) had identical snow samples on the other side of the insulation. By heating the bottoms and cooling the tops, we could maintain similar temperature profiles inside and outside the insulation, thus reducing the driving forces for heat loss from the central snow sample. The narrow ends had a loose insulation composed of styrofoam packing materials outside

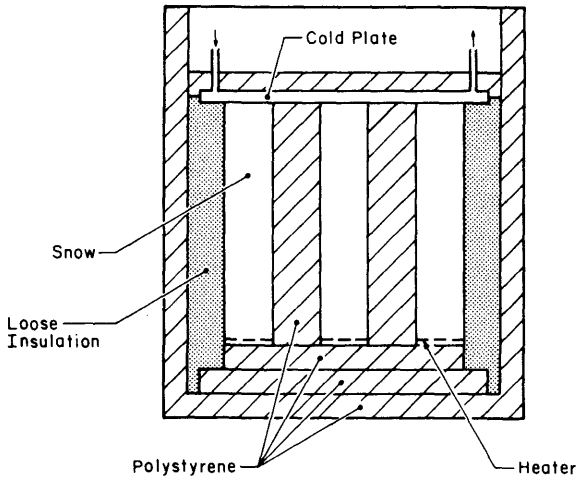

b. Side view.

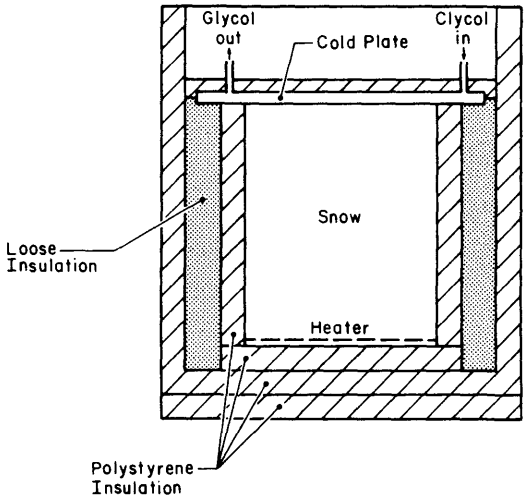

c. Front view.

Figure 23 (cont'd). Apparatus for snow experiments.

the polystyrene slabs. This loose insulation was also cooled on the top and heated on the bottom. Each heater was wired to a separate voltage source, so that temperature profiles in each snow sample could be matched as closely as possible. However, only the central snow sample was used for data collection.

The top boundary for the snow experiments was an aluminum cooling plate through which cold glycol flowed (Fig. 24). In essence, the cooling plate was a rectangular box, with internal dimensions of about 50 by 50 cm by 2 cm deep. The glycol was cooled by a copper coil through which the refrigerant flowed. The glycol was kept at a constant temperature by using a small heater with an on-off temperature controller.

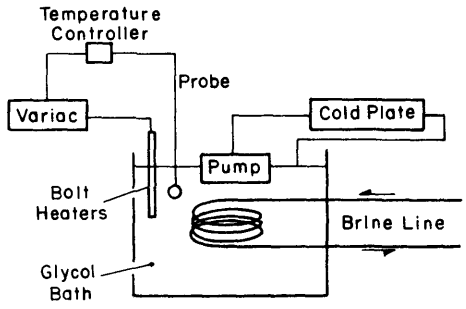

Figure 24. Glycol supply system for the snow experiments.

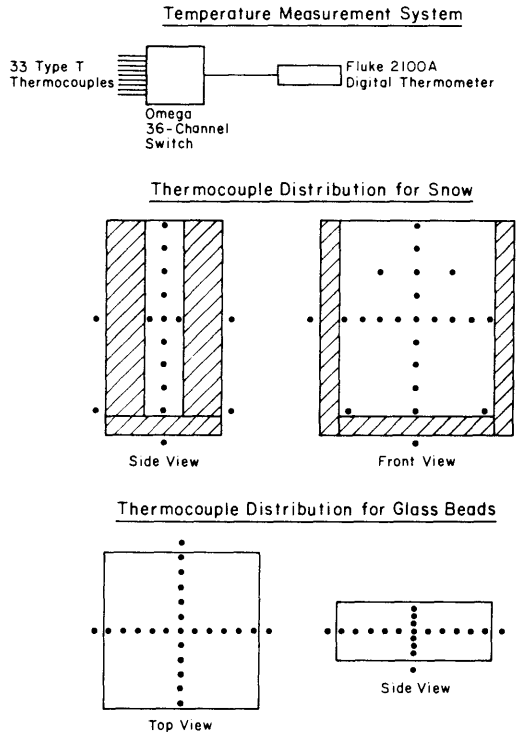

Figure 25. Temperature measurement apparatus and thermocouple placement.

Control of the glycol temperature was good enough to eliminate cyclic temperature variations at the top snow surface.

The temperature measurement system (Fig. 25) consisted of 33 copper-constantan (Type T) thermocouples, wired to a 36-position switch that fed a Fluke digital thermometer (accuracy ±0.1°C). Thermocouples were distributed in the central snow sample as illustrated in Figure 25. Their accuracy was verified using an ice-water bath between each experiment. In each check, the thermocouples read either -0.1° or -0.2°C. Probably a slight offset existed in the Fluke but the offset was not significant since we were mostly interested in temperature differences. The uncertainty in the thermocouple measurements was taken as ±0.1°C, which is negligible.

From the experimental data we calculated the net vertical heat flux through and effective thermal conductivity of each sample. A plot of effective thermal conductivity versus net heat flux has the same physical meaning as a plot of Nusselt number versus Rayleigh number when the Rayleigh number is based on a flux boundary condition. The dimensional form is used for clarity.

In these experiments the temperature profiles and the heat input at the bottom boundary were measured directly. If no heat was lost through the boundaries of the experiment, then the net vertical heat flux was simply the heat input per unit area. However, heat did flow through the sidewalls. These lateral heat flows must be accounted for in the calculation of the net vertical heat flux but the accuracy of the computation is limited by the knowledge we have of the temperature distributions inside and outside the sidewalls.

Lateral heat flows were calculated using the temperature difference across the midpoint of the insulation. If the vertical temperature profiles inside and outside the sidewalls are both linear, then the temperature difference across the sidewall also varies linearly with height so that the average temperature difference is that at the midpoint. Unfortunately, we have no means to deduce how close the profiles were to linear and thus the maximum value of the uncertainty in the heat flux calculation was taken to be the total calculated heat flux through the sidewalls.

The net heat flux was calculated by adding all heat losses or gains to the heat input, and then dividing by the area available for vertical heat flow. The effective thermal conductivity was calculated by dividing the net heat flux by the average gradient across the entire sample. A sample calculation that illustrates this procedure is given in Appendix C.

EXPERIMENTAL RESULTS AND DISCUSSION

Glass beads

To compare the numerical results with the experimental results, we must know the physical properties of each fluid and porous medium. The necessary properties of the bead compact are the thermal conductivity k_m and the intrinsic permeability K. The values of thermal conductivity from the Luikov et al. (1968) model are in close agreement with those measured by Bau (1980), and thus that model is a useful tool in our work.

Permeabilities may be estimated from the Carmen-Kozeny relationship (Wallis 1969)

$$K = \frac{d^2}{180}\left[\frac{\epsilon^3}{(1-\epsilon)^2}\right] \tag{54}$$

where d is a mean particle diameter and ϵ the porosity. Bau (1980) measured permeabilities for the same glass beads used here and found that this relation describes permeabilities well. Calculated parameters for our experiments are listed in Table 4.

Table 4 lists temperature-dependent fluid properties and a product as it appears in the Rayleigh number. The values at 50°C and 30°C for air and water are used in the current discussion and, later, the effects of temperature-dependent fluid properties are discussed.

The essence of the experimental and theoretical results with glass beads is shown in Figures 26a and b, which are plots of effective thermal conductivity versus net heat flux. The calculated k_m corresponds to the horizontal line in Figure 26a, and in both cases the agreement with the experiments is excellent. The inflection point in Figure 26b indicates the theoretical onset of convection, with a corresponding increase in the rate of heat transfer. The horizontal lines indicate the region where the heat flux is less than the critical value for the onset of convection. The value of thermal conductivity used in this region is from the model of Luikov et al. (1969) and is tabulated in Table 4. Above the critical heat flux, the effective thermal conductivity is predicted by eq 44, which is a result from our numerical model.

The critical heat flux is calculated using the theory of convection in porous media presented in the *Background–Porous Media* section. The Rayleigh number was earlier defined as (eq 5)

$$\mathrm{Ra} = \frac{\rho_o \beta g \Delta T H K}{\mu \kappa}$$

Table 4. Physical properties for glass bead experiments.

Saturating fluid	k_f *(cal/cm s °C)*	ϵ	k_m* *(cal/cm s °C)*	K† *(cm²)*
Air	5.35×10^{-5}	0.40	9.62×10^{-4}	2.53×10^{-5}
Water	1.42×10^{-3}	0.44	1.94×10^{-3}	3.77×10^{-5}

*From Luikov et al. (1968).
†Calculated from Carmen-Kozeny relation (eq 54).

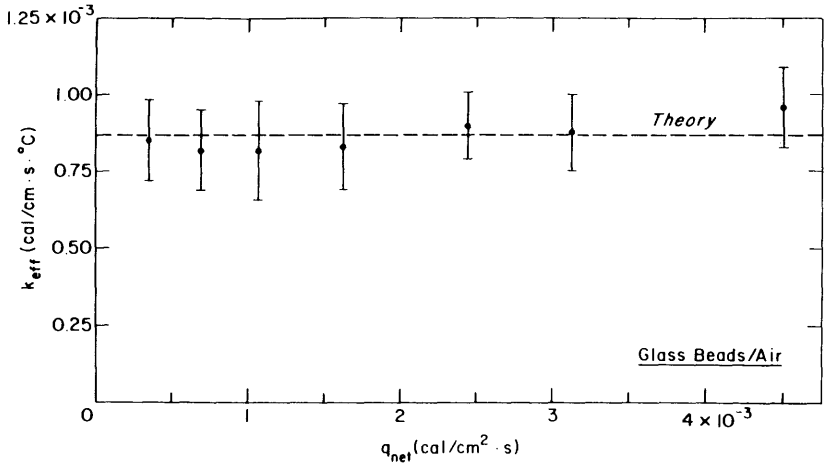

a. Data from experiments are compared with theoretical predictions.

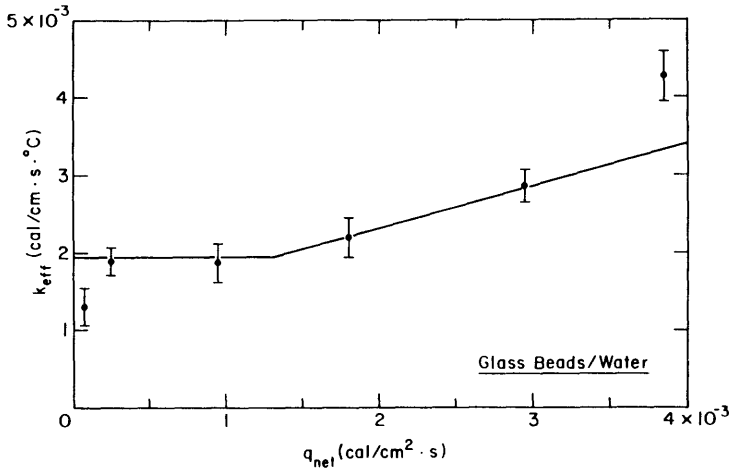

b. Theoretical-numerical results are compared with experimental data from glass beads-water runs.

Figure 26. Effective conductivity versus net vertical heat flux q_{net}.

where

$$\kappa = \frac{k_m}{(\rho C_p)_f} \ .$$

For a constant flux lower boundary, we earlier defined ΔT as qH/k_m. Thus the critical heat flux for the onset of convection is given by

$$q_{cr} = \mathrm{Ra}_{cr} \frac{\mu k_m^2}{\rho_o (\rho C_p)_f \beta g K H^2}. \tag{55}$$

For a constant flux bottom and an isothermal, impermeable top, the critical Rayleigh number is (from Table 1) 27.1 Using k_m and K from Table 4 and fluid properties from Table 5, we

Table 5. Properties of air and water.

$T(^\circ C)$	$\rho_f (g/cm^3)$*	$\mu_f (g/cm\ s)$*	$\beta (^\circ C^{-1})$†	$(\partial V/\partial T)_p$** $(^\circ C^{-1})$	P†† $(cal\ s/cm^5\ 0^\circ C)$	P*** $(cal\ s/cm^5\ ^\circ C^2)$
			Air			
-20	1.40×10^3	1.61×10^4	3.95×10^3	–	1.15×10^5	–
-10	1.31×10^3	1.67×10^4	3.80×10^3	–	0.98×10^5	–
0	1.29×10^3	1.72×10^4	3.66×10^3	–	0.85×10^5	–
10	1.25×10^3	1.76×10^4	3.53×10^3	–	0.75×10^5	–
20	1.20×10^3	1.81×10^4	3.41×10^3	–	0.65×10^5	–
40	1.13×10^3	1.91×10^4	3.19×10^3	–	0.51×10^5	–
60	1.06×10^3	2.00×10^4	3.00×10^3	–	0.40×10^5	–
80	1.00×10^3	2.09×10^4	3.83×10^3	–	0.32×10^5	–
100	0.95×10^3	2.17×10^4	2.68×10^3	–	0.27×10^5	–
			Water			
10	1.000×10^3	1.310×10^2	–	10.37×10^3	–	12.30×10^2
20	0.998×10^3	1.000×10^2	–	2.00×10^3	–	1.99×10^2
30	0.996×10^3	0.796×10^2	–	2.95×10^3	–	2.32×10^2
40	0.992×10^3	0.653×10^2	–	3.80×10^3	–	2.42×10^2
50	0.988×10^3	0.547×10^2	–	4.57×10^3	–	2.41×10^2
60	0.983×10^3	0.466×10^2	–	5.28×10^3	–	2.34×10^2
70	0.978×10^3	0.404×10^2	–	5.96×10^3	–	2.25×10^2

*Roberson and Crowe (1980)

†Holman (1976)

**Dorsey (1940)–$(\partial V/\partial T)_p = \beta/\rho_f$

††$P = \dfrac{\rho_f^2 \beta C_p}{\mu}$

***$P = \dfrac{\rho_f^3 (\frac{\partial V}{\partial T})_p C_p}{\mu_f}$

get $q_{cr} = 6.2\times10^{-2}$ cal/cm^2 s for air and $q_{cr} = 1.31\times10^{-3}$ cal/cm^2 s for water.

Obviously, q_{cr} for air is well out of the range of the experiments and thus convection is not expected. Since the range of physical property variations with temperature is small compared to the difference between the critical and experimental heat fluxes, there is no need to further consider the temperature dependence of air properties. The discussion of the glass bead-air experiment is thus concluded, having shown that experiment and theory agree well.

For the glass bead and water experiments, choice of the proper temperature is important because the critical heat flux for the onset of convection predicted theoretically is within the range observed experimentally. It is also important because fluid properties vary substantially, especially at low temperatures. The runs at high values of heat flux were conducted with average temperatures in the 25° to 30°C range, outside the temperature range where fluid property variations are most significant. Total temperature differences top to bottom were less than 15°C. Thus we can conclude that our earlier calculation of the critical heat flux is within the range of 5-10%. From Figure 26b we see that our calculated critical heat flux agrees well with the experimental results.

Above the critical Rayleigh number on Figure 26b, agreement between the experiments and the prediction of the numerical model are fair. Discrepancies may be introduced because the model is two-dimensional, while either two-dimensional rolls or three-dimensional hexagons are possible in the experiments. The cell form induced by convection is indicated by the steady-state horizontal temperature profiles at the vertical midpoint. Figure 27 shows these temperature profiles for the data points in which convection appeared to be occurring. Each indicates that a three-dimensional cell existed, with warm fluid rising in the center and cool fluid return-

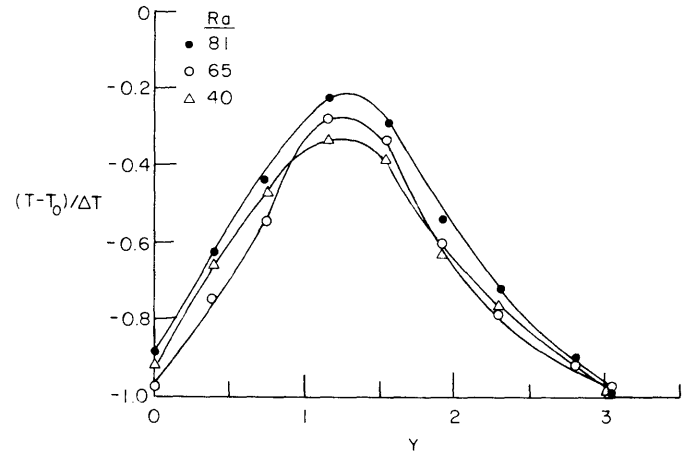

a. y direction profile.

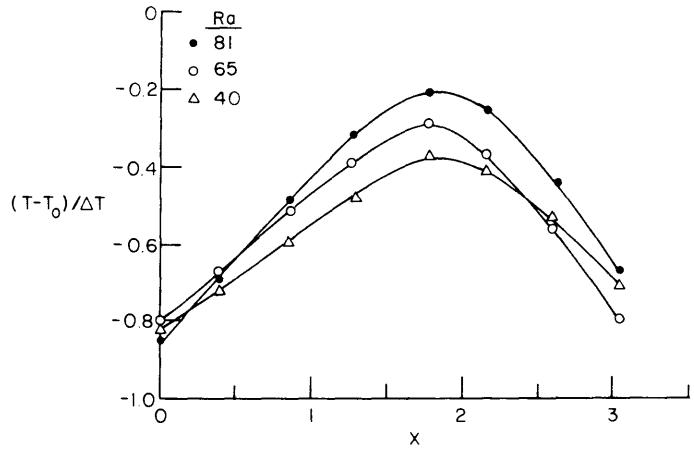

b. x direction profile.

Figure 27. Horizontal temperature profiles for convective heat transfer in experiments with glass beads and water.

ing down the sides. The magnitude of the lateral gradient increases as the Rayleigh number increases, as we would expect for such a cell.

The magnitude of the lateral gradients could be enhanced both by temperature variations on the top plate and by heat losses out the sides. The center of the top plate was always warmer than the edges, and thus the returning fluid lost heat as it passed under the colder outer parts of the plate. By comparing the heat fluxes out the sides with the heat fluxes that would have occurred if the lateral profiles were only attributable to conduction, fluxes out the sides were only about 10% of those calculated by the lateral gradient, and thus must be a relatively small contributor to the lateral temperature profiles.

The three-dimensional convection observed should lead to enhanced gradients near the top and bottom surfaces, and to nearly isothermal conditions in the center. Figure 28 shows the dimensionless centerline temperature profiles for the three convective runs. The data show the expected trend, with the profile becoming more distorted as convection intensifies.

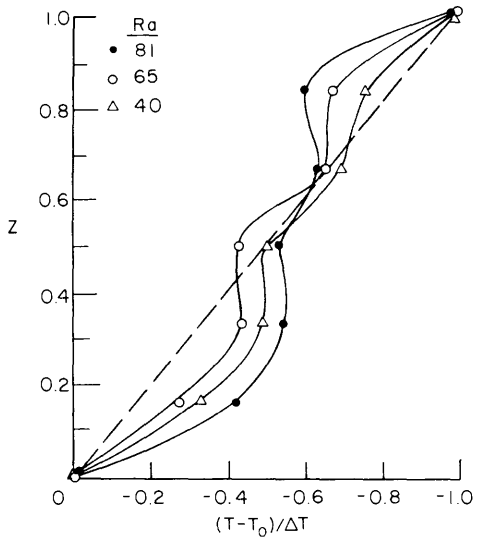

Figure 28. Vertical temperature profiles for convective heat transfer in glass beads and water. Dashed line indicates the pure conduction solution.

Theoretical results for the mode of convection at the onset are not available for the constant flux bottom case. However, Tewari and Torrance (1981) solve for the onset form of convection with an isothermal bottom and permeable top. From Table 1 we see that both the critical Rayleigh number and the critical wave number are identical for the cases of isothermal bottom, permeable top and flux bottom, impermeable top. This is a mathematical consequence of there being one Neumann type (specific gradient) condition for each case. We then expect the form at the onset of convection to be also similar. For the dimensions of the current experiment, Tewari's results indicated that four hexagonal cells should be present. This was certainly not the case with the present experiment. The disagreement may be ascribable to the presence of the lateral heat fluxes discussed earlier. Although not dominant in the heat transfer process, they may be significant enough to alter the form of convection.

From this study with glass beads, three conclusions are apparent. First, that we can induce and reasonably measure convection in porous media. Second, that it is necessary to better control the upper thermal boundary and the heat fluxes through the sides before doing experiments on snow. Third, from a comparison of theoretical-numerical results with the experimental results, we can reasonably conclude that the assumption of a constant flux lower boundary condition was a sound one.

Snow

Results of the snow experiment are shown in Figure 29. Again, effective thermal conductivity is shown as a function of heat flux. We note that the experimental results indicate that con-

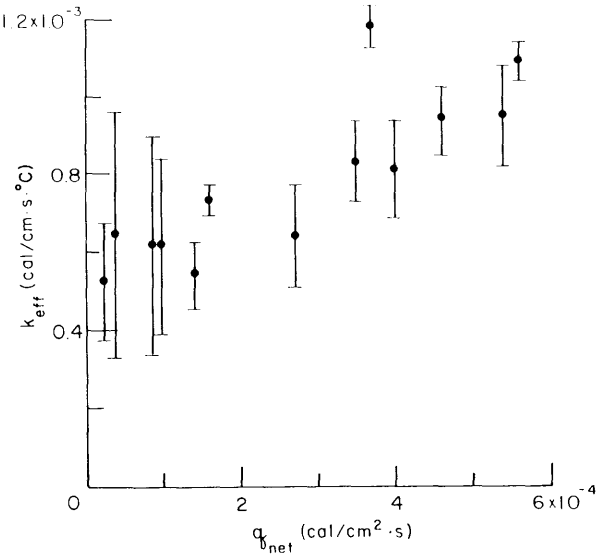

Figure 29. Effective thermal conductivity versus net vertical heat flux. Experimental data from snow experiments.

vection does occur, with a value of critical heat flux of around 1.8×10^{-4} cal/cm^2 s. Calculation of the critical Rayleigh number for the onset of convection is difficult for snow, primarily because of uncertainty in the permeability. Thermal conductivity was measured in our experiments and thus poses no real problem.

A survey of the snow at the start of the experiment revealed an average grain size of about 1.5 mm. The snow used was from the bottom 5 cm of the snow cover, beneath a thick crust. The large grains were formed by wet snow metamorphism followed by dry metamorphism because of strong temperature gradients. The original snow layer was very permeable, as the grain clusters formed by the wet snow metamorphism were still evident, although weakly bonded together. Observations of the snow at the end of the experiment indicated that there was no significant grain growth during the experiment.

The sample was prepared by disaggregating the grain clusters and carefully filling the box, so as to maintain as low a density as possible. Although care was taken, the snow in the box appeared much less permeable than the layer outside. The density was 0.25 g/cm^3.

There is much uncertainty over the intrinsic permeability of snow. Shimizu (1970) proposed the formula

$$K = 0.077d^2 \exp(-7.8\,\rho_s/\rho_w) \tag{56}$$

for snow of mean diameter less than 1 mm. Shimizu measured the permeability of coarse-grained snow at densities of 0.4 g/cm^3 or higher, and found a range of permeabilities of about 2.6×10^{-5} to 5.1×10^{-5} cm^2. Bader (1939) measured permeabilities for coarse-grained snow and depth hoar over the density range of our interest. He found $0.85\times10^{-4} < K < 1.36\times10^{-4}$ cm^2 for coarse-grained snow, and $2.0\times10^{-4} < K < 2.5\times10^{-4}$ cm^2 for depth hoar. Shimizu, however, believed that Bader's experimental technique overestimates permeabilities. Finally, if we extrapolate Shimizu's formula to our case we calculate a permeability of 2.5×10^{-4} cm^2. This coincides with Bader's upper bound, and thus is taken as the upper limit in this experiment. A lower limit is probably in the range of 1.0×10^{-4} cm^2 since Colbeck and Anderson's (1982) data suggest a permeability of 1.4×10^{-4} cm^2 for our snow density.

Fluid properties are given in Table 4 and a thermal conductivity of 6.25×10^{-4} cal/cm s °C is estimated from the heat flow data. Using the properties of air at -20°C, the lowest critical heat flux that we calculate is $q_{cr} = 1.59\times10^{-3}$ cal/cm s. This is about a factor of 6 greater than the observed onset point, a large discrepancy, especially for a lower bound. This apparently results from a large error in the calculated permeability, which is not too surprising considering the uncertainty in permeability discussed above.

The temperature profiles shown in Figure 30 represent two cases where the thermal conductivity (Fig. 31) suggests that convection is occurring, and one case where it suggests that convection is not occurring. The lateral profile for the case without convection in Figure 30a shows a drop near the boundaries, but this may simply be caused by a slight displacement of these thermocouples. In any case the lateral temperature differences are too small compared to the error to draw any conclusions. From the vertical profiles in Figure 30b, we see a temperature profile that is characteristic of the centerline of a single longitudinal roll (see Fig. 2). One roll would also be expected from the theoretical results of Tewari and Torrance (1981). When lateral heat fluxes of the order observed in the experiment are included in our numerical model, we find that only very near the critical Rayleigh number will the cellular form consist of two units. This could be the case for the one experimental run shown here in which we did not expect convection. This Rayleigh number is the one nearest the estimated onset point in Figure 31. The model predicts that close to the critical Rayleigh number, the influence of convection on heat transfer is minimal. The presence of convection is hard to deduce solely from the temperature profiles.

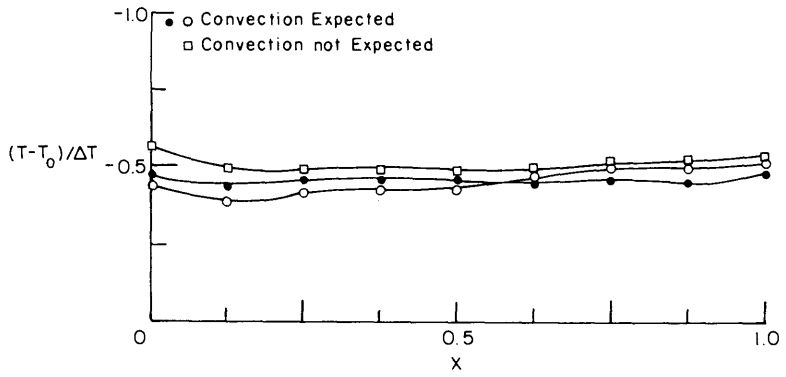

a. Lateral profiles.

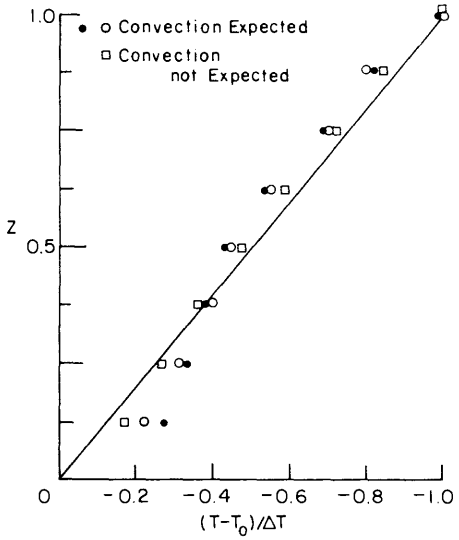

b. Vertical profiles. Solid line indicates the conduction solution.

Figure 30. Temperature profiles for experiments with snow for two runs where convection occurred and one where it did not.

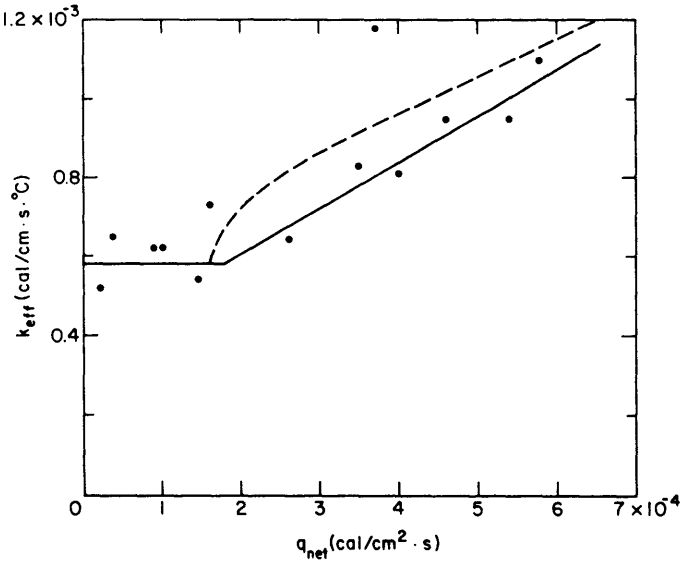

Figure 31. Effective thermal conductivity versus net heat flux. Solid line represents results of numerical model without phase change. Dashed line represents numerical results including phase change with D_{eff} equal to 0.05 cm^2/s.

APPLICATIONS AND CONCLUSIONS

In this section, the aim is to use what we have learned to determine the consequences of convection in snow. The treatment is an introduction to what may be done with our present understanding of convection through snow.

We will focus on two topics. First, the theoretical treatment of the onset of convection is applied to natural snow covers in an attempt to determine just how common convection is under existing conditions. Second, some approaches to modeling snow metamorphism under convective conditions are introduced.

Onset of Benard convection in seasonal snow covers

Previously, we developed the theoretical basis for predicting the onset of Benard convection, based on the value of the Rayleigh number and the boundary conditions. This development allows the prediction of the onset for either horizontal or sloped layers. Rayleigh convection will occur for any inclined snow cover with an applied gradient. We calculated the critical conditions for the onset of convection, and then indicated how common Benard convection might be under naturally occurring conditions.

The Rayleigh number is defined in eq 5. Properties of the snow cover appear as the snowpack depth H, the temperature difference based on boundary conditions ΔT, the intrinsic permeability K and the thermal conductivity of the porous medium k_m. The remaining parameters are temperature-dependent fluid properties or constants. For air, we use properties at typical conditions of -15°C and 10^5 Pa ($\simeq$1 atm) from Table 5. The Rayleigh number is then

$$\mathrm{Ra} = 0.0105 \frac{\Delta THK}{k_m}$$

In the *Effects of Phase Change on Convection* section, we showed that the correct thermal conductivity to use was k_m, or that based on conduction only, i.e., not an effective conductivity that includes vapor diffusion. We ignored both diffusive and convective phase change terms that gave the same results as incorporating both components when the Lewis number is 1.0, a reasonable approximation for low density, dry snow. Later in this section we will further discuss effects of phase change on the onset of convection.

Unfortunately, no data are available that clearly delineate the contributions of conduction and diffusion to the heat transfer process. In the *Heat Transfer* section, we estimated the contribution of vapor diffusion to the effective thermal conductivity as about 2.5×10^{-4} cal/cm s °C for a value of the diffusion coefficient (proposed by Yosida 1955) of 0.85 cm^2/s. In alpine areas where the growth of depth hoar is common, a usual snowpack density is about 0.25 g/cm^3 (Giddings and LaChapelle 1962). Effective thermal conductivity data compiled by Mellor (1977) show that for this density, effective thermal conductivities range from 2.5×10^{-4} to 6.0×10^{-4} cal/cm s °C. The pure conduction conductivity is then probably around 2.5×10^{-4} cal/cm s °C.

For an arbitrary grain size of 1 mm, and a density of 0.25 g/cm^3, Shimizu (1970) predicts a permeability of 1.1×10^{-4} cm. For a snow cover 100 cm deep, the critical temperature difference necessary for the onset of convection is

$$\Delta T_{cr} = 1.73\ \mathrm{Ra}_{cr}\ ^\circ\mathrm{C}\ .$$

The critical Rayleigh number is a function only of boundary conditions (ignoring phase change effects). The soil/snow interface is relatively impermeable and the top boundary is normally permeable, although a wind or rain crust can reduce its permeability. The top boundary is in contact with air that is very nearly at a constant temperature, thus the top snow boundary is nearly

isothermal. It is not known at this point whether the bottom boundary condition is a constant temperature or a constant flux condition, and thus both will be considered. Applying the results from Table 1, we find the critical temperature difference

$$\Delta T_{cr} = \begin{cases} 30.6^{\circ}\mathrm{C} & \text{constant flux bottom} \\ 46.9^{\circ}\mathrm{C} & \text{isothermal bottom} \end{cases}$$

While temperature differences of 30°C may occur in alpine areas, they are certainly not common, and thus this analysis would indicate that Benard type convection is probably not important in alpine areas. In this analysis we have chosen values of the thermal conductivity and permeability based on our best estimates of field conditions.

In subarctic regions, such as interior Alaska, convection is more likely. Trabant and Benson (1972) report that snow densities are frequently around 0.2 g/cm^3, and that by late winter the snow cover can be composed primarily of depth hoar crystals. These may be as large as 1 cm. Typical snow covers are 50-80 cm deep, and are commonly subjected to temperature differences of 30°C. Although we have no permeability or thermal conductivity data for this region, it is likely that the ratio of permeability to thermal conductivity is greater than for alpine snow covers by at least an order of magnitude. This result indicates that convection may be common in regions, such as interior Alaska, where large temperature gradients are imposed upon the snowpack. We take these conclusions as tentative pending the acquisition of better data on permeability and conductivity.

In this discussion, we have not accounted for the effects of phase change, layering or slope. Phase change can raise or lower the critical temperature difference necessary for the onset of Benard convection. For a conductivity of 2.0×10^{-4} cal/cm s °C, the Lewis number is 1.0 when the macroscopic diffusivity is 0.61 cm^2/s and phase change has no effect on the onset of Benard convection. If the diffusivity is higher, as Yen (1963) and Yosida (1955) have observed, the onset of convection is at a higher temperature difference than we earlier calculated and vice versa at lower diffusivities. For a diffusivity of 0.22 cm^2/s, that of water vapor through air, and probably a lower bound, the effect is to lower the critical temperature difference about 10%. If the diffusivities found by Yen and Yosida are correct, the effect of phase change on the onset of convection is to increase the critical temperature difference by less than 10%.

The effects of layering are harder to quantify but are probably not negligible. However, in the theoretical analysis, we used properties of snow that are conducive to the onset of convection. Thus any layering effect would have a negative impact on convection. The exception to this is when there are significant depth hoar layers, in which case the permeability of individual layers can be substantially greater than the permeability used above. If the only layering is that ascribable to the growth of depth hoar layers, then convection may be more likely than we have indicated.

The onset of Benard convection in sloped layers is given by (see the *Convection is Sloped Layers* section)

$$\mathrm{Ra}_{cr} = \frac{\mathrm{Ra}_{cr,o}}{\cos\phi}$$

where $\mathrm{Ra}_{cr,o}$ is the critical Rayleigh number for a horizontal layer. Thus Benard convection is less likely in a sloped layer than in a horizontal layer. In alpine areas it is very unlikely; while in interior Alaska it is probably still common, since even for slopes of 30° the increase in the critical temperature difference is only about 16%. However, it is important to remember that Rayleigh convection, a single cell pattern flowing parallel to the slope, is important in all regions.

Applications to snow metamorphism

Snow metamorphism is a process of crystal growth, the complex interaction of heat removal from and mass transfer to a crystal with the kinetics of phase change at the crystal surface. In this section, we concentrate on the mass transfer process, that is, on the means by which vapor is transported from vapor source to sink, introducing various theoretical means of assessing the importance of convection to the mass transfer process. This section is really more of a literature review than new work; its intent is to point the way for future workers.

Colbeck (1983) assesses the effects of convection in terms of a ventilation factor, the amount by which the mass growth rate is increased because of flow. This approach was developed by cloud physicists as a means of assessing the influence of fall velocity on crystal growth rates (see Prupacher and Klett [1978] for a thorough review). Although results vary somewhat, depending on which correlation for the ventilation factor is used, in general it is safe to say that only at velocities of about 1 cm/s or greater will the influence be substantial.

From Figure 14 we can see that a typical dimensionless maximum velocity for Rayleigh numbers just above the critical value is about 4.0. The scaling factor is κ/H, or $k_m/(\rho C_p)_f H$, where typical values are k_m of 2.5×10^{-4} cal/cm s °C, ρ_f of 1.36×10^{-3} g/cm^3, C_p of 0.24 cal/g °C and H of 100 cm. Then the dimensional velocity is w = 0.04 cm/s. This is approximately the same velocity that results from solving eq 52 for Ra = 10.0 and an angle of 30°, and thus is a good choice as a typical velocity for use in estimating the effects of either Benard or Rayleigh convection.

Obviously, a velocity of 0.04 cm/s is well below that which the ventilation factor approach suggests is important in mass transfer to a particle. However, it is not certain that the ventilation factor approach is a valid one. The key parameter in describing flow around a particle is the Reynolds number, defined as

$$\mathrm{Re} = \frac{\rho_f v d}{\mu_f} \tag{57}$$

where v is the undisturbed velocity. Reynolds numbers for flow around falling snow particles are frequently in the range 1.0–10.0, large enough so that a laminar boundary layer develops. The thickness of this boundary layer (which decreases with increasing Reynolds number) controls the rate of mass transfer. The boundary layer is best thought of as the distance over which mass must diffuse to get from the free stream concentration to the surface concentration. Thus, as the boundary layer thickness decreases, the rate of mass transfer increases.

For thermal convection through snow, velocities are low enough so that the flow may be described as creeping flow, in which viscous terms are important everywhere. The boundary layer has no meaning in creeping flow situations (in effect, the boundary layer thickness is infinite), and thus the boundary layer solutions should tell little about mass transfer during convection through snow.

The effects of creeping flow on mass transfer to a single sphere have been solved by Acrivos and Taylor (1962). Their results indicate that

$$\mathrm{Sh} = 1 + \frac{\mathrm{Pe}}{4} + \frac{\mathrm{Pe}^2}{8} \ln \mathrm{Pe} + 0.03404\ \mathrm{Pe}^2 + 0(\mathrm{Pe}^3) \tag{58}$$

for Pe < 1.0, where Pe is the Peclet number, defined as vd/D, where d is the particle diameter and D the diffusion coefficient. In a rough sense, the Peclet number is the ratio of convective to diffusive contributions. The Sherwood number Sh is similar to a ventilation coefficient. It describes the actual increase in mass transfer when flow is added to the diffusion. For the velocities described above, however, Peclet numbers are small and this solution predicts that flow has little impact on mass transfer.

Intuitively, it would seem that almost any convection would have an important impact on the transfer of mass, given the slow rate at which vapor is transferred by diffusion. A simple method of comparing macroscopic convective and diffusive fluxes is by examining the ratio

$$\frac{v\rho_v}{D_{eff}\dfrac{\partial\rho_v}{\partial T}\dfrac{dT}{dz}} .$$

For common values of dT/dz of 0.2°C/cm and v of 0.04 cm/s, this ratio is about 10, indicating that convection is very important in the overall mass transfer process. This analysis says nothing about what happens to individual grains, only about how much mass is transferred through the snow.

The previous discussions indicate that while convection is important in moving vapor, it only moves vapor past particles and has little impact on crystal growth. Thus, even when convection occurs, snow metamorphism is controlled by the rate of local mass transfer. However, it seems unreasonable to conclude that an order of magnitude increase in macroscopic mass flux leads to no increase in local mass flux, so perhaps our means of quantifying mass transfer to a particle are inadequate.

The above methods for describing the rates of mass transfer to a particle under convective-diffusion conditions assume that the flow near the particle is entirely forced convection, that is, that the transfer processes near the particle have little effect on the flow field. Donaghey (1980) established the following criteria for the transition from forced to mixed free convection:

$Gr/Re^2 < 0.3$	forced convection
$0.3 < Gr/Re^2 < 16$	mixed convection
$16 < Gr/Re^2$	free convection

where Gr is the Grashof number, defined as $\rho_f^2 \beta g \Delta T L^3/\mu_f^2$. By defining the characteristic length L as one particle diameter and defining the temperature difference as this length times an average temperature gradient, we find that the Grashof number is about 0.055. For a velocity of 0.04 cm/s, the Reynolds number is about 0.03, and thus the ratio Gr/Re is about 6. This indicates that even over the limited range of one crystal diameter, buoyancy forces are important in adequately describing the flow field.

To fully analyze the effects of convection on snow metamorphism, it would seem to be necessary to solve the fully coupled mass, energy and momentum equations around a particle. Because of the complex geometries and mathematics, this is a formidable task, which can be addressed only by numerical methods.

Finally, we note the experimental work of Keller and Hallet (1982) on ice crystal growth in a convective environment. Although the supersaturations and velocities used were several orders of magnitude greater than what we expect in snow, their results may be applicable. A key conclusion of theirs was that even in the lower ranges of velocities investigated, the introduction of any flow could change the crystal form from a solid type (plates, columns) to a skeletal type (dendrites, needles). This transition took place even when the change in the growth rate was small. They attributed the skeletal forms to enhanced vapor density gradients along the crystal face, which leads to more rapid growth near corners. This suggests that the onset of convection in some way may coincide with the onset of the growth of hollow crystals.

SUMMARY

The purpose of this work was to investigate thermally driven flows through snow. Toward this end, a numerical model was constructed and experiments were performed on snow and glass beads.

The starting point of the investigation was a theory developed to describe flows through porous media in general. Extensions of the theory were made using a numerical model that accounts for boundary conditions of particular interest for the study of snow. Simple relations were developed, based on the results of the model, which can be used to predict heat transfer based on the choice of the lower thermal boundary condition and the specification of the parameter Ra/Ra_{cr}. The relations are valid for either permeable or impermeable upper boundaries. For the case of an isothermal lower boundary, the results fit existing experimental data as well or better than analytical results. For a constant flux lower boundary, the results of our experiments agree well with the present numerical calculations.

Latent heat terms accounting for phase change between water vapor and ice are included in a unique energy equation used in the numerical model. These terms were found to be significant, especially at the low Rayleigh numbers of interest for snow. The phase change term can intensify or weaken convection, depending on the ratio of the macroscopic diffusivity to the thermal conductivity of the snow. Phase change terms also have a small effect on the conditions for the onset of convection.

Convection in sloped layers was also examined numerically. It was found that misunderstandings existed in previous works dealing with convection in a sloped, porous layer. Here it is found that the intensity of convection is not just a function of the parameter $Ra \cos\phi$ but that lateral confinement plays a very significant role. A physical explanation is offered that consistently explains the observed results in terms of a transition from Benard type convection to Rayleigh type convection.

Analytical solutions were developed to describe the velocity field for convection in a sloped layer with a permeable top at low Rayleigh numbers. The analytical solution agrees well with the numerical model. The importance of layering on convection in sloped layers at low Rayleigh numbers is qualitatively explained.

Experiments indicate that there is natural convection through snow. Because of uncertainties in the permeability, it was necessary to calibrate the modeling by inferring the critical heat flux value from the observed onset of convection. Except for this one problem, agreement between theory and experiment was good. The permeability implied by the critical heat flux we selected is different from that which we would expect based on the few reported values in the literature. This points to an obvious need for further experimental work on the physical properties of snow, especially permeability.

The existing theory for the onset of convection in porous media was applied to two different field settings. We found that convection is unlikely in the alpine regions of the North American Rockies, but is likely to be very common in subarctic regions such as interior Alaska. Simple, unicellular convection in sloped snowpacks is expected in both regions.

Finally, simple theories to describe the effects of convection on snow metamorphism were introduced and applied. For velocities calculated from the modeling results, we found that convection should have little effect on snow crystal growth. However, convection was found to have a substantial effect on the transfer of vapor through the snow cover. It seems possible that thermal convection may not substantially increase the rate of metamorphism but might trigger the growth of the more spectacular hollow crystals with scrolls and striations.

RECOMMENDATIONS

In this work, the means by which a fairly complete understanding of convection in snow might be achieved are developed. However, definitive conclusions cannot be made because we lack a good quantitative understanding of many fundamental processes in and properties of snow.

Foremost among these gaps is a lack of knowledge of just how much vapor is transferred through snow by diffusion. In essence, we do not know the macroscopic (effective) diffusivity of water vapor through snow. Simple experiments done 20 or 30 years ago constitute our entire knowledge. These results supply hints, but in many ways seem inconsistent with our present understanding of vapor transfer through snow.

Related to our lack of understanding of mass transfer through snow, but with further complications of its own, is the subject of heat transfer. At present, our knowledge of thermal conductivity is limited to widely scattered data on effective thermal conductivity, which lump together conduction through ice, conduction through air and latent heat transfer due to vapor diffusion. Our understanding of the relative contribution of each component is purely speculative. A thorough understanding of how heat is transferred through snow is important not only in macroscopic treatments of snow like this, but also in microscopic descriptions of the snow metamorphism process.

Some understanding of the macroscopic diffusivity of snow could be achieved by measuring effective thermal conductivity as a function of temperature only. In addition, a knowledge of the tortuosity of the ice lattice can be gained by measuring the electrical resistance of snow. By coordinating the two efforts, it is felt that a better understanding of heat transfer through snow is possible. Calculation of diffusion coefficients might also be possible with some recent models of local vapor transport.

Our knowledge of snow properties in field situations could also be improved. In particular, it would be interesting to see thermal conductivity and permeability measurements done at the same field sites. This could give us a much better idea of the ways the two are related, and allow a more definite statement concerning the frequency with which convection takes place.

As was indicated earlier, these experiments on convection in snow should be extended to test the initial results. It seems important to measure the permeability of the sample, so that more definite conclusions can be made regarding the agreement between experiment and theory. In addition, sensitive experiments are needed to confirm the validity of theories on the role of phase change on convection. The experimental difficulties of doing very accurate heat transfer experiments on snow are apparent and such experiments will require much time and patience.

Finally, experiments aimed at understanding the role of convection in snow metamorphism are needed, along with better theoretical treatments. A fairly simple experiment would be to tilt a sample of snow, so that convection is forced on the system. In this manner, both convection perpendicular to the temperature gradient and convection parallel to the gradient could be studied.

LITERATURE CITED

Acrivos, A. and T.D. Taylor (1962) Heat and mass transfer from single spheres in Stokes flow. *The Physics of Fluids,* **5**(1): 387-394.

Akitaya, E. (1974) Studies on depth hoar. *Low Temperature Science,* Series A, part 26, pp. 1-67.

Bader, H. (1939) In *Snow and Its Metamorphism.* USA Cold Regions Research and Engineering Laboratory, SIPRE Translation 14 (1954), pp. 1-57.

Bau, H.H. (1980) Experimental and theoretical studies of natural convection in laboratory-scale models of geothermal systems. Ph.D. Dissertation, Cornell University.

Beck, J.L. (1972) Convection in a box of porous material saturated with a fluid. *The Physics of Fluids,* **15**: 1377-1383.

Beier, R.A., J. de Riss and H.R. Baum (1983) Accuracy of finite difference methods in recirculating flows. *Numerical Heat Transfer,* **6**: 283-302.

Bird, R.B., W.E. Stewart and E.N. Lightfoot (1960) *Transport Phenomena.* New York: Wiley and Sons.

Bories, S. and M. Combarnous (1973) Natural convection in a sloping porous layer. *Journal of Fluid Mechanics,* **57**(1): 63-79.

Buretta, R.J. and A.S. Berman (1976) Convective heat transfer in a liquid saturated porous layer. *Journal of Applied Mechanics,* **98**: 249-253.

Chan, B.K.C., C.M. Ivey and J.M. Barry (1970) Natural convection in enclosed porous media with rectangular boundaries. *Journal of Heat Transfer,* **2**: 221-275.

Cheng, P. (1978) Heat transfer in geothermal systems. *Advances in Heat Transfer* (T.F. Irvine and J.P. Hartnett, Ed.). New York: Academic Press, pp. 1-105.

Combarnous, M. and S. Bories (1975) Hydrothermal convection in saturated porous media. *Advances in Hydroscience.* Vol. 10 (V.T. Chow, Ed.). New York: Academic Press, pp. 231-307.

Colbeck, S.C. (1982) An overview of seasonal snow metamorphism. *Reviews of Geophysics and Space Physics,* **20**(1): 45-61.

Colbeck, S.C. (1983) Theory of dry snow metamorphism. *Journal of Geophysical Research,* **88**(C9): 5475-5482.

Colbeck, S.C. and E.P. Anderson (1982) Permeability of a melting snow cover. *Water Resources Research,* **18**(41): 904-908.

Donaghey, L.F. (1980) Hydrodynamics of crystal growth. In *Crystal Growth.* 2nd ed. (B.R. Pamplin, Ed.). Oxford: Pergamon Press.

Dorsey, E.N. (1940) *Properties of Ordinary Water Substance.* New York: Rheinhold Publishing Co.

Dullien, F.A.L. (1979) *Porous Media: Fluid Transport and Pore Structure.* New York: Academic Press.

Elder, J. (1967) Steady free convection in a porous medium heated from below. *Journal of Fluid Mechanics,* **27**: 29-48.

Giddings, J.C. and E.R. LaChapelle (1962) The formation rate of depth hoar. *Journal of Geophysical Research,* **67**: 2377-2383.

Holman, J.P. (1976) *Heat Transfer.* New York: McGraw-Hill.

Kaneko, T., M.F. Mohtadi and K. Aziz (1974) An experimental study of natural convection in inclined porous media. *International Journal of Heat and Mass Transfer,* **17**: 485-496.

Keller, V.W. and J. Hallet (1982) Influence of air velocity on the habit of ice crystal growth from the vapor. *Journal of Crystal Growth,* **60**: 91-106.

Klever, N. (1983) Konvection von wasserdampf in schnee? Presented at Internationolen Polartagung, Bomberg, Federal Republic of Germany.

Krantz, W.B., R.J. Ray, T.N. Caine and R.D. Gunn (1983) A model for patterned-ground regularity. *Journal of Glaciology,* **29**: 317-337.

Lapwood, E.R. (1948) Convection of a fluid in a porous medium. *Proceedings of the Cambridge Philosophical Society,* **44**: 508-521.

Luikov, A.V., A.G. Schaskov, L.L. Vasiliev and Yu.E. Fraimen (1968) Thermal conductivity of porous systems. *International Journal of Heat and Mass Transfer,* **11**: 117-140.

Marbouty, D. (1980) An experimental investigation of temperature gradient metamorphism. *Journal of Glaciology,* **26**(94): 303-312.

McKibben, R. and M.J. O'Sullivan (1980) Onset of convection in a layered porous medium heated from below. *Journal of Fluid Mechanics,* **96**(2): 375-393.

McKibben, R. and M.J. O'Sullivan (1981) Heat transfer in a layered porous medium heated from below. *Journal of Fluid Mechanics,* **111**(1): 141-173.

Mellor, M. (1977) Engineering properties of snow. *Journal of Glaciology,* **19**(81): 32-54.
Neher, J. (1939) In *Snow and Its Metamorphism*. USA Cold Regions Research and Engineering Laboratory, SIPRE Translation 14 (1954), pp. 229-244.
Nield, D.A. (1968) Onset of thermohaline convection. *Water Resources Research,* **4**(3): 553-560.
Palm, E. and M. Tveitereid (1979) On heat and mass flux through dry snow. *Journal of Geophysical Research,* **84**(C2): 745-749.
Palm, E., J.E. Weber and O. Kvernvold (1972) On steady convection in a porous medium. *Journal of Fluid Mechanics,* **54**(1): 153-161.
Pinder, G.F. and W.G. Gray (1977) *Finite Element Simulation in Surface and Subsurface Hydrology.* New York: Academic Press.
Pitman, D. and B. Zuckerman (1967) Effective thermal conductivity of dry snow at -88, -27 and -5°C. *Journal of Applied Physics,* **38**: 2698-2699.
Pruppacher, H.R. and J.D. Klett (1978) *Microphysics of Clouds and Precipitation.* Boston: Reidel Co.
Rana, R., R.N. Horne and P. Cheng (1979) Natural convection in a multilayered porous medium heated from below. *Journal of Heat Transfer,* **101**: 411-416.
Ribando, R.J. (1977) Geothermal energy related problems of natural convection in porous media. Ph.D. Dissertation, Cornell University.
Richard, J.P. and J. Gounot (1981) Critere D'apparition de la convection dans des couches poreuses stratifiees. *International Journal of Heat and Mass Transfer,* **24**(8): 1325-1334.
Roberson, J.A. and C.T. Crowe (1980) *Engineering Fluid Mechanics.* Boston: Houghton Mifflin Co.
Scheidegger, A.E. (1974) *The Physics of Flow Through Porous Media.* Toronto: University of Toronto Press.
Schneider, K.J. (1963) Investigation of the influence of free convection on heat transfer through granular material. In *Proceedings of International Congress on Refrigeration, Munich,* paper 11-4.
Shimizu, H. (1970) Air permeability of deposited snow. *Low Temperature Science,* Series A, Part 22, pp. 1-32.
Straus, J.M. and G. Schubert (1979) Three-dimensional convection in a cubic box of fluid saturated porous media. *Journal of Fluid Mechanics,* **91**(1): 155-165.
Tewari, P.K. and K.E. Torrance (1981) Onset of convection in a box of fluid saturated porous material with a permeable top. *Physics of Fluids,* **24**(5): 981-983.
Trabant, D. and C. Benson (1972) Field experiments on the development of depth hoar. *Geological Society of America,* Memoir 135, pp. 309-322.
Wallis, G. (1969) *One-dimensional Two Phase Flow.* New York: McGraw-Hill.
Weber, J.E. (1975) Convection in a porous medium with horizontal and vertical temperature gradients. *International Journal of Heat and Mass Transfer,* **17**: 241-248.
Yen, Y.C. (1963) Heat transfer by vapor transport in ventilated snow. *Journal of Geophysical Research,* **68**(4): 1093-1101.
Yosida, Z. (1955) Physical studies on deposited snow: 1. Thermal properties. *Low Temperature Science,* Series A, Part 1, pp. 19-74.

APPENDIX A: DERIVATION OF FINITE DIFFERENCE FORMULAE

Constant flux bottom (Fig. A1)–no phase change

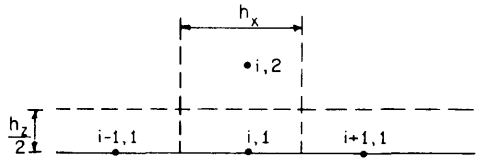

Figure A1. Control volume at lower boundary.

$$\text{Accumulation} = (T_{i,1}^{\ell+1} - T_{i,1}^{\ell})\frac{h_x h_z}{2}$$

$$\text{Conduction} = \frac{(T_{i-1,1} - T_{i,1})}{h_x}\frac{h_z}{2}\Delta t + \frac{(T_{i+1,1} - T_{i,1})}{h_x}\frac{h_z}{2}\Delta t$$

$$+ \frac{(T_{i,2} - T_{i,1})}{h_z} h_x \Delta t + 1\, h_x \Delta t$$

$$\text{Convection} = (uT)_{i-\frac{1}{2}}\frac{h_z}{2}\Delta t - (uT)_{i+\frac{1}{2}}\frac{h_z}{2}\Delta t - (wT)_{1+\frac{1}{2}} h_x \Delta t.$$

Final form:

$$\frac{(T_{i,1}^{\ell+1} - T_{i,1}^{\ell})}{\Delta t} = \frac{(T_{i+1,1} - 2T_{i,1} + T_{i-1,1})}{h_x^2} + 2\frac{(T_{i,2} - T_{i,1})}{h_z^2} + \frac{2}{h_z}$$

$$- \frac{((uT)_{i+\frac{1}{2}} - (uT)_{i-\frac{1}{2}})}{h_x} - \frac{(wT)_{j+\frac{1}{2}}}{h_z}.$$

Constant flux bottom–adiabatic side corner (Fig. A2)

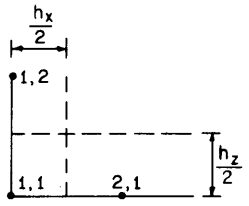

Figure A2. Control volume at left corner of lower boundary.

$$\text{Accumulation} = (T_{1,1}^{\ell+1} - T_{1,1}^{\ell})\frac{h_x h_z}{4}$$

$$\text{Conduction} = \frac{(T_{2,1} - T_{1,1})}{h_x} \frac{h_z}{2} \Delta t + \frac{(T_{1,2} - T_{1,1})}{h_z} \frac{h_x}{2} \Delta t + \frac{h_x}{2} \Delta t$$

$$\text{Convection} = -(uT)_{i+\frac{1}{2}} \frac{h_z}{2} \Delta t - (wT)_{j+\frac{1}{2}} \frac{h_x}{2} \Delta t$$

Final form:

$$\frac{(T_{1,1}^{\ell+1} - T_{1,1}^{\ell})}{\Delta t} = 2 \frac{(T_{2,1} - T_{1,1})}{h_x^2} + 2 \frac{(T_{1,2} - T_{1,1})}{h_z^2} + \frac{2}{h_z}$$

$$- 2 \frac{(uT)_{i+\frac{1}{2}}}{h_x} - 2 \frac{(wT)_{j+\frac{1}{2}}}{h_z} .$$

Opposite corner, final form:

$$\frac{(T_{nx,1}^{\ell+1} - T_{nx,1}^{\ell})}{\Delta t} = 2 \frac{(T_{nx-1,1} - T_{nx,1})}{h_x^2} + 2 \frac{(T_{nx,2} - T_{nx,1})}{h_z^2}$$

$$+ \frac{2}{h_z} + 2 \frac{(uT)_{nx-\frac{1}{2}}}{h_x} - 2 \frac{(wT)_{1-\frac{1}{2}}}{h_z} .$$

Formula for calculating Nusselt numbers for isothermal boundaries

For these calculations, we assume steady state–bottom boundary (see Fig. A1):

Accumulation = 0

$$\text{Conduction} = \frac{(T_{i+1,1} - T_{i,1})}{h_x} \frac{h_z}{2} \Delta t + \frac{(T_{i-1,1} - T_{i,1})}{h_x} \frac{h_z}{2} \Delta t - \left(\frac{\partial T}{\partial z}\right)_i h_x \Delta t + \frac{T_{i,2} - T_{i,1}}{h_z} h_x \Delta t.$$

$$\text{Convection} = (uT)_{i-\frac{1}{2}} \frac{h_z}{2} \Delta t - (uT)_{i+\frac{1}{2}} \frac{h_z}{2} \Delta t - (wT)_{1+\frac{1}{2}} h_x \Delta t.$$

Final form:

$$\left(\frac{\partial T}{\partial z}\right)_i = \frac{(T_{i+1,1} - 2T_{i,1} + T_{i-1,1})}{h_x^2} \frac{h_z}{2} + \frac{(T_{i,2} - T_{i,1})}{h_z}$$

$$- ((uT)_{i+\frac{1}{2}} - (uT)_{i-\frac{1}{2}}) \frac{h_z}{2h_x} - (wT)_{1+\frac{1}{2}} .$$

Top boundary, final form:

$$\left(\frac{\partial T}{\partial z}\right)_i = - \frac{(T_{i+1,nz} - 2T_{i,nz} + T_{i-1,nz})}{h_x^2} \frac{h_z}{2} - \frac{(T_{i,nz-1} - T_{i,nz})}{h_z}$$

$$+ ((uT)_{i+\frac{1}{2}} - (uT)_{i-\frac{1}{2}}) \frac{h_z}{2h_x} - (wT)_{nz-\frac{1}{2}} .$$

Bottom corners (see Fig. A2):

Accumulation = 0

$$\text{Conduction} = \frac{(T_{2,1} - T_{1,1})}{h_x}\,\frac{h_z}{2}\Delta t + \frac{(T_{1,2} - T_{1,1})}{h_z}\,\frac{h_x}{2}\Delta t - \left(\frac{\partial T}{\partial z}\right)_1 \frac{h_x}{2}\Delta t$$

$$\text{Convection} = -(uT)_{1+\frac{1}{2}}\,\frac{h_z}{2}\Delta t - (wT)_{1+\frac{1}{2}}\,\frac{h_x}{2}\Delta t\,.$$

Final form:

$$\left(\frac{\partial T}{\partial z}\right)_1 = (T_{2,1} - T_{1,1})\,\frac{h_z}{h_x^2} + (T_{1,2} - T_{1,1})\,\frac{1}{h_z} - (uT)_{1+\frac{1}{2}}\,\frac{h_z}{h_x} - (wT)_{1+\frac{1}{2}}\,.$$

Opposite corner, final form:

$$\left(\frac{\partial T}{\partial z}\right)_{nx} = (T_{nx-1,1} - T_{nx,1})\,\frac{h_z}{h_x^2} + (T_{nx,2} - T_{nx,1})\,\frac{1}{h_z}$$

$$+ (uT)_{nx-\frac{1}{2}}\,\frac{h_z}{h_x} - (wT)_{1+\frac{1}{2}}\,.$$

Top corners, final form, $i = 1$:

$$\left(\frac{\partial T}{\partial z}\right)_1 = -(T_{2,nz} - T_{1,nz})\,\frac{h_z}{h_x^2} - (T_{1,nz-1} - T_{1,nz})\,\frac{1}{h_z}$$

$$+ (uT)_{1+\frac{1}{2}}\,\frac{h_z}{h_x} - (wT)_{nz-\frac{1}{2}}\,.$$

Top corners, final form, $i = nx$:

$$\left(\frac{\partial T}{\partial z}\right)_{nx} = -(T_{nx-1,nz} - T_{nx,nz})\,\frac{h_z}{h_x^2} - (T_{nx,nz-1} - T_{nx,nz})\,\frac{1}{h_z}$$

$$- (uT)_{nx-\frac{1}{2}}\,\frac{h_z}{h_x} - (wT)_{nz-\frac{1}{2}}\,.$$

The Nusselt number is then given by:

$$\text{Nu} = \frac{\sum_{i=1}^{nx}\left(\frac{\partial T}{\partial z}\right)_i h_{x_i}}{\sum_{i=1}^{nx} h_{x_i}} = \frac{h_x\left(\left(\left(\frac{\partial T}{\partial z}\right)_1 + \left(\frac{\partial T}{\partial z}\right)_{nx}\right)/2 + \sum_{i=2}^{nx-1}\left(\frac{\partial T}{\partial z}\right)_i\right)}{\text{AR}}$$

Formula for calculating Nusselt number for constant flux boundaries

$$\text{Nu} \equiv ((T_{bot} - T_{top})_{av})^{-1} = \left(\sum_{i=1}^{nx} h_{x_i}(T_{i,1} - T_{i,nz})\right)^{-1}\,.$$

APPENDIX B: COMPUTER PROGRAMS

Main program

```
C         PROGRAM TO CALCULATE THERMAL CONVECTION FLOWS IN POROUS MEDIUM
C
C         DIMENSION ARRAYS
C
      DIMENSION T(75,21),PSI(75,21),SPARE(75,21),U(75,21),W(75,21)
      DIMENSION SOURCE(75,21)
      DIMENSION A(75),B(75),C(75),R(75)
C
C         DEFINE ARRAYS
C
C         T: TEMPERATURE
C         PSI: STREAM FUNCTION
C         SPARE: SPARE FIELD, USED IN CALCULATIONS FOR BOTH PSI AND T
C         U: X DIRECTION VELOCITY (HORIZONTAL)
C         W: Y DIRECTION VELOCITY (VERTICAL)
C         SOURCE: RIGHT HAND SIDE OF MOMENTUM EQUATION
C         A,B,C COEFFICIENTS OF IMPLICIT FD FORM
C         R RIGHT HAND SIDE OF IMPLICIT FD FORM
C
C         DEFINE CONSTANTS
C
C         CM:   SOR RELAXATION FACTOR
C         HX:   GRID SPACING IN X DIRECTION
C         HZ:   GRID SPACING IN Z DIRECTION
C         NX:   NUMBER OF NODES IN X DIRECTION
C         NZ:   NUMBER OF NODES IN Z DIRECTION
C         ASRAT:   ASPECT RATIO, HOR./VERT.
C         THETA:   ANGLE OF TILT, FROM HORIZONTAL
C         CONVER:   CONVERGENCE REQUIREMENT FOR ITERATIVE
C                   SOLUTION OF STREAMFUNCTION EQUATION.
C         DELT:   TIME STEP
C         RA: RAYLEIGH NUMBER
C         PERT: VALUE OF INITIAL TEMPERATURE DISTRIBUTION
C         NITER: ITERATION NUMBER IN ADI ITERATIVE
C         NT: TIME STEP NUMBER
C
C         READ CONSTANTS
C
      PRINT 70
      READ (1,*) RA
      PRINT 72
      READ (1,*) NX
      PRINT 82
      READ (1,*) NZ
      PRINT 83
      READ (1,*) ASRAT
      PRINT 84
      READ (1,*) THETA
      PRINT 74
      READ (1,*) DELT
      PRINT 75
      READ (1,*) IFILE
      IF (IFILE.NE.1) GOTO 15
      PRINT 76
      PRINT 77
      READ (1,*) FSEQ
 15   PRINT 78
      READ (1,*) IPRINT
      IF (IPRINT .NE. 1) GOTO 16
      PRINT 81
      READ (1,*) PSEQ
 16   PRINT 79
      READ (1,*) IPSI
      PRINT 80
      READ (1,*) ITEMP
 76   FORMAT ('INPUT SEQ: (I.E. IF SEQ=5,EVERY FIFTH TIME STEP')
 77   FORMAT ('WILL GENERATE RESULTS THAT ARE FILED')
 78   FORMAT ('INPUT IPRINT, IPRINT=1 WILL PRINT RESULTS')
 79   FORMAT ('INPUT IPSI, IPSI=1 GIVES PERMEABLE TOP')
 80   FORMAT ('INPUT ITEMP, ITEMP=1 GIVES CONSTANT FLUX BOTTOM')
 81   FORMAT ('INPUT PSEQ: HOW OFTEN RESULTS ARE PRINTED')
 82   FORMAT ('INPUT NZ, NUMBER OF NODES IN Z DIRECTION')
 84   FORMAT ('INPUT THETA,ANGLE OF TILT FROM HOR. IN DEGREES')
 83   FORMAT ('INPUT ASPECT RATIO (HORIZONTAL/VERTICAL)')
 74   FORMAT ('INPUT DELTA T, TIME STEP')
 75   FORMAT ('INPUT IFILE, IF=1, RESULTS WILL BE FILED')
 70   FORMAT ('INPUT RAYLEIGH NUMBER')
 71   FORMAT ('NOTE THAT BOTH X AND Z NUMBERS OF NODES')
 73   FORMAT ('MUST MATCH THOSE OF THE INPUT FILES')
```

```
 72     FORMAT ('INPUT NX, NUMBER OF NODES IN X DIRECTION')
        HX=ASRAT/(NX-1)
        HZ=1./(NZ-1)
        AR=HZ/HX
        THETA=THETA*3.14159/180.
        ARSQ=AR**2.
        NT=0
        PERT=1.E-2
        NZM=NZ-1
        NXM=NX-1
        OM=1.7
        CONVER=1.E-4
        IWRIT=31
C
        DO 10 J=1,NZ
           TLEV=-HZ*(J-1)
           DO 10 I=1,NX
              T(I,J)=TLEV
 10     CONTINUE
C
C      TEMP PERTURBATION TO START FLOWS
C
        T(NX,2)=T(NX,2)+PERT
C
C      START CALCULATIONS HERE
C
        MT=2
        IF (ITEMP.EQ.1) MT=1
        MP=NZM
        IF (IPSI.EQ.1) MP=NZ
C
 100    NT=NT+1
        PRINT 62,NT
        NITER=0
        CZ=DELT/(2.*HZ**2)
        CX=DELT/(2.*HX**2)
C
C      CALCULATE SOURCE TERM
C
        DO 20 J=2,NZM
        DO 20 I=2,NXM
           SOURCE(I,J)=RA*AR*(T(I+1,J)-T(I-1,J))*HZ*COS(THETA)/2.
     !              -RA*HZ*SIN(THETA)*(T(I,J+1)-T(I,J-1))/2.
 20     CONTINUE
C
C         SET SPARE FIELD TO ZERO AT BOUNDARIES
C            FOR SOLUTION OF STREAMFUNCTION EQUATION
C
        DO 21 J=1,NZ
           SPARE(1,J)=0.0
           SPARE(NX,J)=0.0
 21     CONTINUE
        DO 22 I=1,NX
           SPARE(I,1)=0.0
           SPARE(I,NZ)=0.0
 22     CONTINUE
C
C       DO FOR PERMEABLE TOP ONLY
C
        IF (IPSI.NE.1) GOTO 102
        DO 23 I=2,NXM
           SOURCE(I,NZ)=RA*(HZ/2.)*(COS(THETA)*AR*(T(I+1,NZ)-T(I-1,NZ))
     !                 -SIN(THETA)*(3.*T(I,NZ)-4.*T(I,NZM)+T(I,NZ-2)))
 23     CONTINUE
C
C      ADI-SOR STEPS     CALCULATE PSI UNTIL ADEQUATE CONVERGENCE
C
C           STEP 1, IMPLICIT IN X
C
 102    NITER=NITER+1
        DIFFMX=0.0
        PSIMAX=0.0
        PSIMIN=0.0
        DO 30 J=2,MP
           DO 32 I=2,NXM
              A(I-1)=ARSQ
              B(I-1)=-2.*ARSQ-OM
              C(I-1)=ARSQ
              IF (J.NE.NZ) GOTO 5
              R(I-1)=-2.*PSI(I,NZ-1)+(2.-OM)*PSI(I,NZ)+SOURCE(I,J)
              GOTO 32
 5            R(I-1)=SOURCE(I,J)-PSI(I,J+1)-PSI(I,J-1)+(2.-OM)*PSI(I,J)
 32        CONTINUE
           CALL THOMF (A,B,C,R,NX-2)
           DO 38 I=2,NXM
              SPARE(I,J)=R(I-1)
 38        CONTINUE
 30     CONTINUE
C
C           STEP 2,   IMPLICIT IN Z
```

```
C
      DO 33 I=2,NXM
         DO 34 J=2,MP
            JJ=J-1
            A(JJ)=1.
            B(JJ)=-2.-CM
            C(JJ)=1.
           R(JJ)=SOURCE(I,J)-ARSQ*(SPARE(I+1,J)+SPARE(I-1,J)
     !      -2.*SPARE(I,J))-CM*SPARE(I,J)
   34    CONTINUE
         A(NZM)=2.
    6    CALL THOMF (A,B,C,R,MP-1)
         DO 35 J=2,MP
            JJ=J-1
            DIFF=ABS(R(JJ)-PSI(I,J))
            IF (DIFF.GT.DIFFMX) DIFFMX=DIFF
            PSI(I,J)=R(JJ)
            IF (PSI(I,J).GT.PSIMAX) PSIMAX=PSI(I,J)
            IF (PSI(I,J).LT.PSIMIN) PSIMIN=PSI(I,J)
   35    CONTINUE
   33 CONTINUE
C
C     CALCULATE CONVERGENCE
C
      CRIT=DIFFMX/(ABS(PSIMAX)+ABS(PSIMIN)+0.01)
      IF (CRIT.GT.CONVER) GOTO 102
      PRINT 120, PSIMAX,PSIMIN
  120 FORMAT ('PSIMAX=',E12.4,3X,'PSIMIN=',E12.4)
      PRINT 61,NITER
   67 FORMAT ('NITER=',I4,'CRIT=',E12.4)
C
C     CALCULATE VELOCITY FIELD
C
      DO 36 I=2,NXM
         DO 37 J=2,NZM
            U(I,J)=-(PSI(I,J+1)-PSI(I,J-1))/(2.*HZ)
            W(I,J)=(PSI(I+1,J)-PSI(I-1,J))/(2.*HX)
   37    CONTINUE
         U(I,1)=-(4.*PSI(I,2)-3.*PSI(I,1)-PSI(I,3))/(2.*HZ)
         U(I,NZ)=-(-4.*PSI(I,NZM)+3.*PSI(I,NZ)+PSI(I,NZ-2))/(2.*HZ)
   36 CONTINUE
      DO 31 J=2,NZM
         W(1,J)=(4.*PSI(2,J)-3.*PSI(1,J)-PSI(3,J))/(2.*HX)
         W(NX,J)=(-4.*PSI(NXM,J)+3.*PSI(NX,J)+PSI(NX-2,J))/(2.*HX)
   31 CONTINUE
C
      IF (IPSI.NE.1) GOTO 103
      DO 39 I=2,NXM
         W(I,NZ)=(PSI(I+1,NZ)-PSI(I-1,NZ))/(2.*HX)
   39 CONTINUE
      W(1,NZ)=(4.*PSI(2,NZ)-3.*PSI(1,NZ)-PSI(3,NZ))/(2.*HX)
      W(NX,NZ)=(3.*PSI(NX,NZ)-4.*PSI(NXM,NZ)+PSI(NX-2,NZ))/(2.*HX)
C
C     NOW CALCULATE TEMPERATURE FIELD
C      USING NON ITERATIVE ADI AS A TIME STEPPING MEANS
C
C     IMPLICIT IN X
C
  103 DO 40 J=MT,NZM
         DO 41 I=1,NX
            IF (J.EQ.1) GOTO 7
            WP=(W(I,J+1)+W(I,J))/2.
            WM=(W(I,J-1)+W(I,J))/2.
            R(I)=T(I,J+1)*CZ*(2.-HZ*(WP-ABS(WP)))
     !     +T(I,J)*(1.-CZ*(4.+HZ*(WP+ABS(WP)-WM+ABS(WM))))
     !     +T(I,J-1)*CZ*(2.+HZ*(WM+ABS(WM)))
            GOTO 8
    7       WP=W(I,2)/2.
            R(I)=T(I,2)*CZ*2.*(2.-HZ*(WP-ABS(WP))) +
     !           T(I,1)*(1.-CZ*(4.+2.*HZ*(WP+ABS(WP)))) +
     !           4.*CZ*HZ
    8       IF (I.EQ.1) GOTO 3
            IF (I.EQ.NX) GOTO 4
            UP=(U(I+1,J)+U(I,J))/2.
            UM=(U(I-1,J)+U(I,J))/2.
            A(I)=CX*(-2.-HX*(UM+ABS(UM)))
            B(I)=1.+CX*(4.+HX*(UP+ABS(UP)-UM+ABS(UM)))
            C(I)=CX*(-2.+HX*(UP-ABS(UP)))
            GOTO 41
    3       UP=U(2,J)/2.
            B(1)=1.+CX*(4.+2.*HX*(UP+ABS(UP)))
            C(1)=CX*(-4.+2.*HX*(UP-ABS(UP)))
            GOTO 41
    4       UM=U(NX-1,J)/2.
            A(NX)=CX*(-4.-2.*HX*(UM+ABS(UM)))
            B(NX)=1.+CX*(4.-2.*HX*(UM-ABS(UM)))
   41    CONTINUE
   95    FORMAT (E12.4,3X,E12.4,3X,E12.4,3X,E12.4)
C
C
C     SOLVE
```

```
C
            CALL THOMF (A,B,C,R,NX)
            DO 43 I=1,NX
               SPARE(I,J)=R(I)
 96            FORMAT (4X,E12.4)
 43         CONTINUE
 40       CONTINUE
C
C       IMPLICIT IN Z
C
          DO 44 I=1,NX
            SPARE(I,NZ)=-1.0
 44       CONTINUE
          DO 50 I=1,NX
             IF (ITEMP.NE.1) GOTO 9
            WP=W(I,2)/2.
            B(1)=1.+CZ*(4.+2.*HZ*(WP+ABS(WP)))
            C(1)=CZ*(-4.+2.*HZ*(WP-ABS(WP)))
 9          DO 51 J=MT,NZM
               JJ=J-MT+1
               IF (J.EQ.1) GOTO 11
               WP=(W(I,J+1)+W(I,J))/2.
               WM=(W(I,J)+W(I,J-1))/2.
               A(JJ)=CZ*(-2.-HZ*(WM+ABS(WM)))
               B(JJ)=1.+CZ*(4.+HZ*(WP+ABS(WP)-WM+ABS(WM)))
               C(JJ)=CZ*(-2.+HZ*(WP-ABS(WP)))
 11            IF (I.EQ.1) GOTO 1
               IF (I.EQ.NX) GOTO 2
               UP=(U(I,J)+U(I+1,J))/2.
               UM=(U(I,J)+U(I-1,J))/2.
               R(JJ)=SPARE(I+1,J)*CX*(2.-HX*(UP-ABS(UP)))+SPARE(I,J)*
     !               (1.-CX*(4.+HX*(UP+ABS(UP)-UM+ABS(UM)))) +
     !               SPARE(I-1,J)*CX*(2.+HX*(UM+ABS(UM)))
               GOTO 51
  1            UP=U(2,J)/2.
               R(JJ)=SPARE(1,J)*(1.-CX*(4.+2.*HX*(UP+ABS(UP))))+
     !         SPARE(2,J)*CX*(4.-2.*HX*(UP-ABS(UP)))
               GOTO 51
  2            UM=U(NX-1,J)/2.
               R(JJ)=SPARE(NXM,J)*CX*(4.+2.*HX*(UM+ABS(UM)))+
     !         SPARE(NX,J)*(1.+CX*(-4.+2.*HX*(UM-ABS(UM))))
 51         CONTINUE
C
C         FOLLOWING IS FOR CONSTANT HEAT FLUX ONLY
C
             IF (ITEMP.EQ.1) R(1)=R(1)+4.*CZ*HZ
             R(NZ-MT)=R(NZ-MT)-C(NZ-MT)*SPARE(I,NZ)
            DO 53 J=MT,NZM
               JJ=J-1
               IF (MT.EQ.1) JJ=J
 53         CONTINUE
C
C       SOLVE
C
            CALL THOMF (A,B,C,R,NZ-MT)
            DO 52 J=MT,NZM
               T(I,J)=R(J-MT+1)
 52         CONTINUE
 50       CONTINUE
C
C
C
C        NOW PRINT OR FILE IF SO DESIGNATED
C
           IF (IPRINT.NE.1) GOTO 104
           AA=FLOAT(NT)/FSEQ
           BB=INT(NT/FSEQ)
           IF (AA.NE.BB) GOTO 104
           PRINT 65
 65        FORMAT ('VELOCITY FIELD')
           DO 199 J=1,NZ
              M=NZ+1-J
              PRINT 88, W(2,M),W(4,M),W(6,M),W(8,M),W(10,M)
 199       CONTINUE
           PRINT 66
66         FORMAT ('TEMPERATURE FIELD')
           DO 200 J=1,NZ
            M=NZ+1-J
              PRINT 88, T(2,M),T(4,M),T(6,M),T(8,M),T(10,M)
 200       CONTINUE
C
104     IF (IFILE.NE.1) GOTO 105
C
          AA=FLOAT(NT)/FSEQ
          BB=INT(NT/FSEQ)
          IF (AA.NE.BB) GOTO 105
          PRINT 87
 87       FORMAT (' DO YOU WISH TO FILE, YES=1,NO=0')
          READ (1,*) IFILE2
          PRINT 187
 187      FORMAT ('DO YOU WISH TO CHANGE TIME STEP: YES=1')
          READ (1,*) ITIME
          IF (ITIME.NE.1) GOTO 188
```

```
      PRINT 189
 189  FORMAT ('INPUT NEW TIME STEP')
      READ (1,*) DELT
 188  PRINT 190
 190  FORMAT ('DO YOU WISH TO CHANGE RA, YES=1')
      READ (1,*) IRA
      IF (IRA .NE. 1) GOTO 191
      PRINT 192
 192  FORMAT ('INPUT NEW RA')
      READ (1,*) RA
 191  PRINT 193
 193  FORMAT ('DO YOU WISH TO CHANGE ANGLE, YES=1')
      READ (1,*) IANG
      IF (IANG.NE.1) GOTO 195
      PRINT 194
 194  FORMAT ('INPUT NEW ANGLE, IN DEGREES')
      READ (1,*) ANG
      ANG=3.14159/180.
 195  IF (IFILE2.NE.1) GOTO 105
      IWRITP=IWRIT+1
      CALL GFILES (IWRIT,2,'TFILENAME',9)
      CALL GFILES (IWRITP,2,'PSIFILNM',8)
      DO 1000 I=1,NX
         WRITE (IWRIT,99) (T(I,J) , J=1,NZ)
         WRITE (IWRITP,99) (PSI(I,J) , J=1,NZ)
1000  CONTINUE
      CALL CLOSAL
      IWRIT=IWRIT+2
C
C
C     NOW COMPUTE NUSSELT NUMBERS TOP AND BOTTOM,
C      AND CALCULATE CONVERGENCE BASED ON ENERGY
C      CONSERVATION.
C
C
C      BOTTOM NUSSELT NUMBER
 105  BOTNU=0.0
      DO 59 I=2,NXM
         UP=(U(I+1,1)+U(I,1))/2.
         UM=(U(I-1,1)+U(I,1))/2.
         WP=W(I,2)/2.
         BOTNU=BOTNU-0.5*(AR*(T(I+1,1)+T(I-1,1)-2.*T(I,1))) -
     !                  (T(I,2)-T(I,1))/AR
     !              +(HZ/4.)*(T(I,1)*(UP+ABS(UP)-UM+ABS(UM))
     !          +T(I+1,1)*(UP-ABS(UP)) -T(I-1,1)*(UM+ABS(UM)))
     !              +(HX/2.)*((WP-ABS(WP))*T(I,2)+(WP+ABS(WP))*T(I,1))
 59   CONTINUE
      UP=U(2,1)/2.
      WP=W(1,2)/2.
      BOTNU=BOTNU-0.5*(AR*(T(2,1)-T(1,1))+(T(1,2)-T(1,1))/AR)
     !          +(HZ/4.)*(T(1,1)*(UP+ABS(UP))
     !          + T(2,1)*(UP-ABS(UP))) + (T(1,2)*(WP-ABS(WP))
     !          + T(1,1)*(WP+ABS(WP)))*(HX/4.)
      UM=U(NX-1,1)/2.
      WP=W(NX,2)/2.
      BOTNU=BOTNU-0.5*(AR*(T(NXM,1)-T(NX,1)) +
     !          (T(NX,2)-T(NX,1))/AR) - (HZ/4.)*(T(NXM,1)*
     !          (UM+ABS(UM)) +T(NX,1)*(UM-ABS(UM)))
     !          +(HX/4.)*(T(NX,2)*(WP-ABS(WP))+T(NX,1)*
     !          (WP+ABS(WP)))
C
C          TOP NUSSELT NUMBER
C
      TOPNU=0.0
      DO 60 I=2,NXM
         UP=(U(I+1,NZ)+U(I,NZ))/2.
         UM=(U(I-1,NZ)+U(I,NZ))/2.
         WM=(W(I,NZM)+W(I,NZ))/2.
         TOPNU=TOPNU+0.5*AR*(T(I+1,NZ)+T(I-1,NZ)-2.*T(I,NZ))
     !             +(T(I,NZM)-T(I,NZ))/AR
     !             -(HZ/4.)*(T(I,NZ)*(UP+ABS(UP)-UM+ABS(UM))
     !             +T(I+1,NZ)*(UP-ABS(UP)) - T(I-1,NZ)*(UM+ABS(UM)))
     !             +(HX/2.)*(T(I,NZ)*(WM-ABS(WM))+T(I,NZM)*(WM+ABS(WM)))
 60   CONTINUE
      WM=(W(1,NZM)+W(1,NZ))/2.
      UP=U(2,NZ)/2.
      TOPNU=TOPNU+0.5*(AR*(T(2,NZ)-T(1,NZ))+(T(1,NZM)-T(1,NZ))/AR)
     !     -(HZ/4.)*(T(1,NZ)*(UP+ABS(UP))+T(2,NZ)*(UP-ABS(UP)))
     !     +(HX/4.)*(T(1,NZM)*(WM-ABS(WM))+T(1,NZ)*(WM+ABS(WM)))
      WM=(W(NX,NZM)+W(NX,NZ))/2.
      UM=U(NXM,NZ)/2.
      TOPNU=TOPNU+0.5*(AR*(T(NXM,NZ)-T(NX,NZ)))
     !     +0.5*(T(NX,NZM)-T(NX,NZ))/AR
     !      +(HZ/4.)*(T(NX,NZ)*(UM-ABS(UM)) + T(NXM,NZ)*
     !      (UM+ABS(UM))) + (HX/4.)*(T(NX,NZ)*(WM-ABS(WM))
     !      +T(NX,NZM)*(WM+ABS(WM)))
      TOPNU=TOPNU/ASRAT
      BOTNU=BOTNU/ASRAT
      BAL=(ABS(TOPNU-BOTNU))/ABS(BOTNU)
      PRINT 63, TOPNU,BOTNU,BAL
C
      IF (NT.LT.1000) GOTO 100
```

```
C
C
  61    FORMAT (1X,'NITER=',I5)
  62    FORMAT (5X,'NT=',I5)
  63    FORMAT ('TOPNU=',1X,E12.4,3X,'BOTNU=',1X,E12.4,3X,
     !           'BALANCE=',1X,E12.4)
  88    FORMAT (6(2X,E12.4))
  99    FORMAT (11(E11.4,1X))
        STOP
        END
$INSERT THOMFN
```

Plotting routine

```
C       PROGRAM TO PLOT DATA FILES
C
        DIMENSION D(100,21),X(4),Z(4),CL(4),XPLT(4),ZPLT(4)
C
        PRINT 50
50      FORMAT ('INPUT THETA,ANGLE BETWEEN X AXIS AND HORIZONTAL')
        READ (1,*) THETA
        PRINT 51
  51    FORMAT ('INPUT LENGTH (IN INCHES) OF X,Z AXES')
        READ (1,*) XL,ZL
        CALL PLOTS(0)
        ZMAX=1.
        PRINT 52
        READ (1,*) AR
 52     FORMAT ('INPUT ASPECT RATIO')
        XMAX=AR
        XL=XL/XMAX
        ZL=ZL/ZMAX
        PRINT 60
60      FORMAT ('INPUT NUMBER OF HORIZONTAL NODES')
        READ (1,*) MX
        PRINT 61
61      FORMAT ('INPUT NUMBER OF VERTICAL NODES')
        READ (1,*) MZ
        DELX=XMAX/(MX-1)
        DELZ=ZMAX/(MZ-1)
C
100     PRINT 63
63      FORMAT ('INPUT DATA FILE NAME')
        CALL GFILES (5,1,'FILENAME',8)
C
        PRINT 75
 75     FORMAT ('WHAT COLOR PEN')
        READ (1,*) IPEN
        DO 10 I=1,MX
           READ (5,80) (D(I,J), J=1,MZ)
 10     CONTINUE
        CALL CLOSAL
 80     FORMAT (11(E11.4,1X))
C
C        THIS SECTION SPECIFIES THE RANGE AND DETAIL DESIRED
C        FOR THE PLOT.
C
        DMAX=0.0
        DMIN=0.0
        DO 20 I=1,MX
        DO 20 J=1,MZ
           IF (D(I,J) .GT. DMAX) DMAX=D(I,J)
           IF (D(I,J) .LT. DMIN) DMIN=D(I,J)
 20     CONTINUE
        PRINT 65, DMAX
 65     FORMAT ('MAX VALUE=',1X,E12.4)
        PRINT 66, DMIN
 66     FORMAT ('MIN VALUE=',1X,E12.4)
        PRINT 67
 67     FORMAT ('INPUT MAXIMUM VALUE OF CONTOUR LINE DESIRED')
        READ (1,*) DMAX
        PRINT 68
 68     FORMAT ('INPUT DESIRED MINIMUM VALUE OF CONTOUR LINES')
        READ (1,*) DMIN
        PRINT 69
 69     FORMAT ('INPUT DESIRED NUMBER OF CONTOUR LINES')
        READ (1,*) NLINES
        PRINT 70
 70     FORMAT ('INPUT LINE TYPE: SEE MANUAL FOR LINE TYPE DEF.')
        READ (1,*) ITYPE
C
C      ACTUAL PLOTTING BEGINS HERE
C
C
        DELD=(DMAX-DMIN)/(NLINES-1)
        DPLT=DMIN
        MXM=MX-1
        MZM=MZ-1
        H=ZMAX*ZL
```

```
      CALL NEWPEN(IPEN)
      DO 25 N=1,NLINES
         DO 30 I=1,MXM
         DO 30 J=1,MZM
            X(1)=(I-1)*DELX
            X(2)=I*DELX
            X(3)=X(2)
            X(4)=X(1)
            Z(1)=(J-1)*DELZ
            Z(3)=J*DELZ
            Z(2)=Z(1)
            Z(4)=Z(3)
            DL(1)=D(I,J)
            DL(2)=D(I+1,J)
            DL(3)=D(I+1,J+1)
            DL(4)=D(I,J+1)
            IPLT=1
            DO 31 K=1,4
               KP=K+1
               IF (K.EQ.4) KP=1
               IF ((DPLT.GT.DL(K)) .AND. (DPLT.GT.DL(KP))) GOTO 31
               IF ((DPLT.LT.DL(K)) .AND. (DPLT.LT.DL(KP))) GOTO 31
               POLATE=ABS((DPLT-DL(K))/(DL(KP)-DL(K)))
               XPLT(IPLT)=X(K)*XL
               IF (Z(K).EQ.Z(KP)) XPLT(IPLT)=(X(K)+POLATE*
     !            (X(KP)-X(K)))*XL
               ZPLT(IPLT)=Z(K)*ZL
               IF (X(K).EQ.X(KP)) ZPLT(IPLT)=(Z(K)+POLATE*
     !            (Z(KP)-Z(K)))*ZL
               IPLT=IPLT+1
 31         CONTINUE
            IF (IPLT.EQ.1) GOTO 30
            IF (IPLT.GT.3) GOTO 30
            IF (THETA.EQ.0) GOTO 102
            CALL ANGLE (XPLT(1),ZPLT(1),THETA,H)
            CALL ANGLE (XPLT(2),ZPLT(2),THETA,H)
102         CALL PLOT (XPLT(1),ZPLT(1),3)
            CALL PLOT (XPLT(2),ZPLT(2),ITYPE)
 30      CONTINUE
         DPLT=DPLT+DELD
 25   CONTINUE
C
      PRINT 71
 71   FORMAT (*DO YOU WISH TO PLOT MORE DATA: YES=1*)
      READ (1,*) NPLOT
      IF (NPLOT .EQ. 1) GOTO 100
      PRINT 72
 72   FORMAT (*DO YOU WISH TO PLOT GRID: YES=1*)
      READ (1,*) IGRID
      IF (IGRID .NE. 1) GOTO 101
C
C     PLOT GRID
C
      PRINT 75
      READ (1,*) IPEN
      CALL NEWPEN(IPEN)
      DO 40 J=1,MZ
         X1=0.0
         Z0=(J-1)*DELZ*ZL
         Z2=Z0
         IF (THETA.NE.0) CALL ANGLE (X1,Z2,THETA,H)
         CALL PLOT (X1,Z2,3)
         DO 40 I=2,MX
            X1=(I-1)*DELX*XL
            Z2=Z0
            IF (THETA.NE.0) CALL ANGLE (X1,Z2,THETA,H)
            CALL PLOT (X1,Z2,2)
 40   CONTINUE
C
      DO 41 I=1,MX
         Z1=0.
         X0=(I-1)*DELX*XL
         X2=X0
         IF (THETA.NE.0) CALL ANGLE (X2,Z1,THETA,H)
         CALL PLOT (X2,Z1,3)
         DO 41 J=2,MZ
            Z1=(J-1)*DELZ*ZL
            X2=X0
            IF (THETA.NE.0) CALL ANGLE(X2,Z1,THETA,H)
            CALL PLOT (X2,Z1,2)
 41   CONTINUE
C
C    PLOT BOUNDARIES IF SO DESIRED
C
 101  PRINT 73
 73   FORMAT (*DO YOU WISH TO PLOT BOUNDARIES: YES=1*)
      READ (1,*) IBND
      IF (IBND.NE.1) GOTO 103
      PRINT 75
      READ (1,*) IPEN
      CALL NEWPEN(IPEN)
```

```
      DO 90 J=1,2
         X1=0.0
         IF (J.EQ.1) ZC=0.0
         IF (J.EQ.2) ZC=ZL*ZMAX
         Z2=ZC
         IF (THETA.NE.0) CALL ANGLE (X1,Z2,THETA,H)
         CALL PLOT (X1,Z2,3)
         DO 90 I=2,MX
            X1=(I-1)*DELX*XL
            Z2=ZC
            IF (THETA.NE.0) CALL ANGLE (X1,Z2,THETA,H)
            CALL PLOT (X1,Z2,2)
 90   CONTINUE
C
      DO 91 I=1,2
         Z1=0.0
         IF (I.EQ.1) XC=0.0
         IF (I.EQ.2) XC=XL*XMAX
         X2=XC
         IF (THETA.NE.0) CALL ANGLE (X2,Z1,THETA,H)
         CALL PLOT (X2,Z1,3)
         DO 91 J=2,MZ
            Z1=(J-1)*DELZ*ZL
            X2=XC
            IF (THETA.NE.0) CALL ANGLE (X2,Z1,THETA,H)
            CALL PLOT (X2,Z1,2)
 91   CONTINUE
C
103   CALL PLOT (0.,0.,999)
      STOP
      END
$INSERT ANGLE
```

APPENDIX C: SAMPLE CALCULATIONS

Data from snow experiment 2 February 1984.

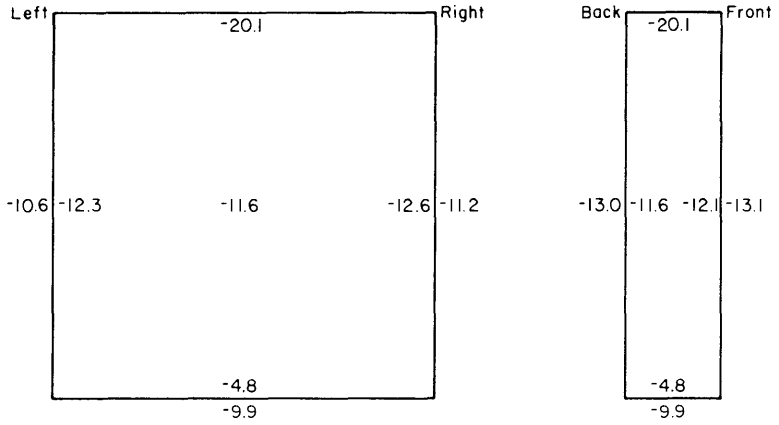

Figure C1. Relative dimensions of snow sample along with measured temperatures (°C).

V = 5.83 V

R = 47.4 Ω

Q_{in} = V^2/R = 0.71 W = 0.1714 cal/s

Side fluxes = (k_{ins}) (area of heat transfer) ($\Delta T/\Delta z$)

k_{ins} is the thermal conductivity of the polystyrene insulation, and is

k_{ins} = 6.2×10^{-5} cal/cm s°C.

Right = $(6.2 \times 10^{-5}) \times (50 \times 10\ cm^2) \times (1.4°C/5\ cm)$ = $+8.47 \times 10^{-3}$ cal/s

Left = $(6.2 \times 10^{-5}) \times (50 \times 10\ cm^2) \times (1.7°C/5\ cm)$ = $+1.03 \times 10^{-2}$ cal/s

Front = $(6.2 \times 10^{-5}) \times (50 \times 40\ cm^2) \times (1.0°C/10\ cm)$ = -1.21×10^{-2} cal/s

Back = $(6.2 \times 10^{-5}) \times (50 \times 40\ cm^2) \times (1.4°C/10\ cm)$ = -1.69×10^{-2} cal/s

sum of side fluxes = -1.02×10^{-2} cal/s

% of input = 0.0102/0.1714 = 5.9%

Bottom = $(6.2 \times 10^{-5}) \times (40 \times 10\ cm^2) \times (5.1°C/10\ cm)$ = -1.26×10^{-2} cal/s

Net heat flow = 0.1714
-0.0102
-0.0126

0.1486 cal/s

net heat flux = net heat flow per area

= 0.1486 cal/s per 400 cm^2

q_{net} = 3.7×10^{-4} cal/cm^2s

effective thermal conductivity (k_{eff}) = $q_{net}/(\Delta T/\Delta z)$

k_{eff} = $3.7 \times 10^{-4}/((-4.8-(-20.1))/50)$

k_{eff} = 1.18×10^{-3} cal/cm s°C.

Uncertainty in k_{eff} is estimated by multiplying fraction heat loss through the sides by the thermal conductivity.

uncertainty in k_{eff} = $(1.18 \times 10^{-3}) \times 0.059 = \pm 6.96 \times 10^{-5}$ cal/cm s°C.